UNIVERSITÀ DEGLI STUDI DI PALERMO
Dottorato in Scienze della Terra e del Mare
Dipartimento di Scienze della Terra e del Mare (Di.S.Te.M)
GEO/08

Zr, Hf and REE fractionation between dissolved pool and sediments in river waters. Effects of changing ionic strength conditions in element partitioning between truly dissolved and colloidal fractions

DOTTORE
Fabio Sposito

COORDINATORE
Prof. Alessandro Aiuppa

TUTOR
Prof. Paolo Censi

CO TUTOR
Dr. Salvatore Inguaggiato

CICLO XXX
2018

UNIVERSITÀ DEGLI STUDI DI PALERMO
Dottorato in Scienze della Terra e del Mare
Dipartimento di Scienze della Terra e del Mare (Di.S.Te.M)
GEO/08

Zr, Hf and REE fractionation between dissolved pool and sediments in river waters. Effects of changing ionic strength conditions in element partitioning between truly dissolved and colloidal fractions

DOTTORE
Fabio Sposito

COORDINATORE
Prof. Alessandro Aiuppa

TUTOR
Prof. Paolo Censi

CO TUTOR
Dr. Salvatore Inguaggiato

CICLO XXX
2018

ABSTRACT

This PhD thesis study examines the aspects concerning the geochemistry of Rare Earth, Zr and Hf in dissolved pools of continental river waters, in relation to the effects that ionic strength can generate in the distribution of the elements among the considered fractions in the aqueous phase: dissolved fraction (DF < 450 nm), colloidal fraction (10 kDa < CF < 450 nm) and the so called "truly dissolved" fraction (TDF < 10 kDa). Furthermore, the behaviour of the same elements was investigated in different bottom sediments fractions: exchangeable and Ca-carbonate, Mn-oxyhydroxides, Fe-oxyhydroxides and residual/silicate.

Since there are few studies concerning the processes regulating these elements fractionation in the considered aqueous pools in hypersaline environments, the research was carried out in the southern central sector of Sicily (Italy), in particular in continental waters of the Platani river basin interacting with thick evaporitic sequences (Upper Miocene) and abandoned landfills derived from historical mining activities. Weathering of evaporites allows to consider the hydrological investigated basin as a natural saline laboratory, where a wide spectrum of ionic strength values is available, from 0.1 to 4.3 mol l^{-1} which allows to classify the analysed waters as brackish, saline and brines.

Ionic strength is one of the main parameters responsible for the stability of the colloids, as increasing values can determine their coagulation in natural waters, as suggested by previous studies conducted in estuarine zones. Coagulation of colloids leads to the REE released from colloidal fraction and their scavenging onto surfaces of suspended particles or their complexation in the truly dissolved phase.

The behaviour of Zr, Hf and REE in the investigated aqueous fractions is determined by the nature and composition of the CF, withstanding as dissolved salts exceed 200 g l^{-1}. The composition of CF consists of suspended material with dimensions in a range of values between 10 kDa and 450 nm, representing the coarser part of the totality of colloids and it is constituted by aggregates of Al-oxyhydroxides, clays particles and lithogenic origin carbonate nanoparticles. The result of this

study indicates that the relative abundance of the colloidal fraction has a double effect: the first, concerning the fractionation of intermediate REEs (enrichment in MREE), visible in the normalized distribution to PAAS (Post Archean Australian Shale) in the DF and the second, represented by different Zr/Hf chondritic signature values (relative to Chondritic reference values) in all considered aqueous pools.

The investigated basin therefore allows evaluating the key role played by ionic strength, whose colloid dependence reveals the fractionation of Zr and Hf, which is realized by the effect of larger Hf affinity with respect to Zr by means of Al-oxyhydroxide surfaces and carbonate nanoparticles. Therefore, the Zr/Hf ratio in the CF shows sub-chondritic values (lower than Chondritic reference rock), caused by the preferential removal of Hf on the solids surfaces, leaving the truly dissolved phase with an excess of Zr compared to Hf, as shown by the super-chondritic values (higher than Chondritic reference rock) of the Zr/Hf ratio.

Carbonate nanoparticles (Mg-calcite and/or dolomite) are also responsible for light positive Gd/Gd* anomalies in DF. Since the highest values were found in those samples where the Mg/Ca molar ratio is close to the unity, the dissolution of the Mg-salts of the mine activities landfill, would not represent a possible source of gadolinium. Values of $Gd/Gd^* > 1$ were also found in CF and TDF, suggesting that the observed positive Gd anomalies are caused by the complete carbonate dissolution in TDF or by carbonatic nanoparticles relict in the colloidal aggregates.

Finally, among the four bottom sediments fractions, those constituting the Exchangeable and Ca-carbonatic and Fe-oxyhydroxide are the only ones where a clear fractionation of the rare earth elements occurs, proved by the middle REE enrichment (MREE). Since the same distribution is also recognized in some samples of the aqueous dissolved phase, it is likely that these two solid fractions may represent a source of MREE in aqueous phase.

RIASSUNTO

Questo studio di tesi di dottorato esamina gli aspetti riguardanti la geochimica delle Terre Rare, Zr e Hf in fase disciolta di acque continentali fluviali, in relazione agli effetti che la forza ionica può generare nella distribuzione degli elementi tra le frazioni considerate in fase acquosa: disciolta (DF < 450 nm), colloidale (10 KDa < CF < 450 nm) e quella denominata "veramente" disciolta (TDF < 10 kDa). Inoltre, il comportamento degli stessi elementi è stato investigato in sedimenti di fondo in diverse frazioni della fase solida: Ca-carbonatica, ossi-idrossidi di Mn, ossi-idrossidi di Fe e frazione residuale/silicatica.

Poiché non esistono studi sui processi che regolano il frazionamento degli elementi considerati nelle frazioni acquose studiate in ambienti iper-salini, la ricerca è stata condotta nel settore centro meridionale della Sicilia (Italia), in particolare nelle acque fluviali del bacino idrologico del fiume Platani che interagiscono con potenti sequenze evaporitiche (Miocene Superiore) e discariche abbandonate derivate da storiche attività minerarie. Il weathering di rocce evaporitiche permette dunque di considerare il bacino idrologico investigato come un laboratorio salino naturale, in cui è disponibile un ampio spettro valori di forza ionica da 0.1 a 4.3 mol l^{-1}, che consente di classificare le acque analizzate come salmastre, saline e brine.

La forza ionica è tra i principali parametri responsabili della stabilità dei colloidi, poiché un suo incremento può determinarne la coagulazione loro nelle acque naturali, come suggerito da studi precedenti condotti in zone estuarine. La coagulazione colloidi può provocare il rilascio delle terre rare e il loro scavenging su superfici di particelle sospese o il loro complessamento nella fase veramente disciolta.

Nel sistema fluviale considerato, il comportamento di Zr, Hf e REE nelle tre frazioni acquose considerate è determinato dalla natura e composizione della CF, capace di resistere alla coagulazione fino a valori di TDS che superano 200 g $l^{-.1}$. La frazione colloidale considerata è costituita da materiale in sospensione con dimensioni in un intervallo di valori compreso tra 10 kDa e 450 nm, rappresenta la fase più grossolana della totalità dei colloidi ed è costituita da aggregati di

ossi-idrossidi di Al, particelle argillose di dimensioni colloidali e nanoparticelle carbonatiche di natura litogenica. Il risultato di questo studio indica che l'abbondanza relativa della frazione colloidale determina un duplice effetto: il primo riguarda il frazionamento delle REE intermedie (arricchimento in MREE), visibile nella distribuzione normalizzata al PAAS (Post Archean Australian Shale) nella DF mentre il secondo riguarda i valori del rapporto molare Zr/Hf diversi rispetto al valore di riferimento condritico.

Il sistema fluviale indagato permette dunque di valutare il ruolo chiave svolto dalla forza ionica, la cui dipendenza dei colloidi svela il frazionamento di Zr e Hf che si attua per effetto di una maggiore affinità per Hf rispetto a Zr per mezzo delle superfici di ossi-idrossidi di Al e delle particelle carbonatiche. Pertanto, il rapporto Zr/Hf nella frazione colloidale mostra valori subcondritici (inferiori rispetto al valore di riferimento della condrite), causati dalla preferenziale rimozione di Hf sulle superfici dei solidi, lasciando la fase veramente disciolta con un eccesso di Zr rispetto a Hf, come mostrano dai valori supercondritici (maggiori rispetto al valore di riferimento della condrite) del rapporto Zr/Hf.

Le nanoparticelle carbonatiche (Mg-calcite e/o Dolomite) sono inoltre responsabili di anomalie positive di Gd/Gd* di lieve entità nella DF; poiché i valori più elevati sono calcolati nelle acque in cui il rapporto molare Mg/Ca è intorno all'unità, la dissoluzione dei sali di Mg, derivati dalla lisciviazione del materiale di risulta della miniera Bosco Palo, non rappresenterebbe una possibile sorgente di gadolinio. Valori di Gd/Gd* > 1 sono stati riscontrati nella CF e nella TDF, suggerendo che l'origine di questa anomalia è legata alla dissoluzione dei carbonati nella TDF o a nanoparticelle carbonatiche relitte negli aggregati colloidali.

Infine, tra le quattro frazioni analizzate dei sedimenti di fondo, quelle costituenti la frazione Ca-carbonatica e quella a agli ossi-idrossido di Fe, sono le uniche in cui avviene un chiaro frazionamento degli elementi delle terre rare, visibile attraverso un arricchimento nelle REE intermedie (MREE). Poichè questa stessa distribuzione è riconoscibile anche in alcuni campioni

della fase disciolta, è verosimile che queste due frazioni solide analizzate rappresentino una sorgente di MREE in fase acquosa.

Table of contents

List of figures

List of Tables

CHAPTER 1

INTRODUCTION

General aspects and aim of the research

The rare earth elements (lanthanides and yttrium) are natural important resources, with an increasing exploitation in the last 30 years, used in technology and in generic electronic devices for their quality as excellent electrical conductors. REE, Zr and Hf were previously considered as immobile elements and free from geochemical fractionations during water-rock interaction. The evolution of analytical techniques, mainly derived by ICP-MS allowed the progressively REE investigation at more and more lower concentrations in dissolved phase. This permitted to develop an extensive literature in the 40 years, about the distribution of REE, during interaction process between different phases while very limited investigation were carried out on Zr and Hf geochemical behaviour. Investigation on Zr and Hf in natural process started about 20 years ago and they were focused mainly in seawater Zr and Hf fractionation.

These first studies were mainly set on the REE, Zr and Hf capability to provide insights into geochemical processes occurring in natural environments (Wood, 1990; Bau, 1996; Koschinsky and Hein, 2003; Bau and Dulski, 1999) as seawater (McKlivey and Orians, 1993; 1998; Godfrey et al., 1996; Firdaus et al., 2009) and continental waters (De Carlo and Green, 2002; Kerrich et al 2002; Tang and Johannesson, 2006; Bau and Koschinsky, 2006; Godfrey et al., 2008; Gonzalez-Alvarez and Kerrich, 2010; Vazquez-Ortega et al., 2015) in a wide range of temperature, pH, Eh and salinity. These researches were mainly focused on REE, Zr and Hf distribution in order to demonstrate the role played by natural waters as carrier of trace element from Continents to Ocean (Goldstein and Jacobsen, 1988; Elbaz-Poulichet and Dupuy, 1999; Sholkovitz and Szymczak, 2000). The importance of studying isovalent elements defined geochemical twins as Zr-Hf and Y-H in waters and their fractionation processes involving solid phases is given by their different

behaviour in aqueous solution respect to high temperature silicate melts where fractionaction processes are mainly controlled by the ion charge and radius. Different behaviour is observed in aqueous solutions, where Y/Ho and Zr/Hf ratios deviate from chondritic ratio, due to fractionation processes ruled also by their electronic configurations (Bau, 1996).

In river waters REE, Zr and Hf are distributed between three different fractions: suspended particulate matter, colloidal particles and solution phases and their relative competition determines the extent of the fractionation (Sholkovitz, 1992). Since these metals are strong particle-reactive elements, they are usually associated to the colloidal fraction that usually represents REE, Zr and Hf main carrier (Sholkovitz, 1993; 1995; Lawrence and Kamber, 2006; Johannesson et al., 2017).

In this study salinity play an important role, since it could be considered a key function driving the REE, Zr and Hf release to the truly dissolved fraction or their scavenging by the bottom sediments (Bau and Koschinsky, 2006), depending on surface/solution reactions (Sholkovitz, 1995). This process, was already investigated by several studies regarding only REE behaviour, whereas few data sets are available on the Zr and Hf distribution between colloidal and truly dissolved fraction in continental waters affected by high saline contents. Furthermore, just few studies are available concerning colloidal fraction in high saline waters, so it is unknown if colloids persist at ionic strength similar or higher to seawater and the eventual chemical composition. Very recently, Merschel et al. (2017) suggested that the coagulation of colloids induced by salinity growth in estuarine zones is a phenomenon working differently on colloidal stability as a function of colloids composition.

Because of the lack of knowledge about colloids stability at high salinity, this PhD research investigated the nature and composition colloidal fraction up to 10 KDa (10 KDa < CF < 450 nm) occurring in natural system where ionic strength values attains above 4 mol kg^{-1}. The above-mentioned chemical conditions were recognized in the Platani river catchment basin (about 2000 km^2 wide), characterised by wide spread evaporitic outcropping rocks belonging to the Gessoso-Solfifera Formation (Upper Miocene sequences). Weathering of evaporites and waste deposit of

abandoned mining activities produces salt waters in two main tributaries of Platani basin: Gallo d'Oro and Salito River. The described natural system, characterised by rural condition with low anthropic impact, was considered a natural geochemical lab with suitable conditions for investigating REE, Zr and Hf concentrations in continental waters under a wide range of ionic strength. Furthermore, particular attention was focused on the investigation of the distribution of these elements among three different water fractions: dissolved (DF), 10 KDa colloidal (CF) and truly dissolved (TDF). The same investigation was conducted on authigenic fraction of river bottom sediments with particular interest on the distribution of REE, Zr and Hf in four fractions of sediment: exchangeable cations and Ca carbonates, easily reducible, moderately reducible and residual fraction.

1.2 Aqueous geochemistry of REE

Rare Earth Elements are a group of 15 elements belonging to the f-block and arbitrarily they could be split in three groups: light (La, Ce, Pr, Nd, Pm), middle (Sm, Eu, Gd, Tb, Dy), heavy (Ho, Er, Tm, Yb, Lu). All these elements have quite similar chemical properties, due to their changing external electronic configuration from La to Lu, expressed by the filling of the inner 4f orbitals. This is their main feature and the progressive filling of the 4f orbitals closer to the nucleus, induces a phenomenon called "Lanthanide contraction", consisting in the progressive decrease of ionic radius with the increasing atomic number (Shannon, 1976).

In natural waters rare earth elements are predominant in solution with the trivalent oxidation state, whereas tetravalent cerium and bivalent europium could be also find in oxidized and reduced state, respectively. Compared to Ho, Y is characterized by the similar ionic radius and same oxidation (+3) and although the lacking of f-electrons, it could be included in the HREE (Heavy Rare Earth Elements) group. According to the *Refined Spin-pairing Energy Theory (RSPET)*

(Nugent, 1970), suggesting the existence of a direct relationship between the electronic configuration and chemical equilibrium, sometimes REE normalized pattern and/or distribution coefficients could be split into four different curves called *Tetrads*.

The REE could form complexes with several inorganic ligands: carbonate, hydroxide, sulphate, chlorine, fluorine, phosphate (Wood, 1990; Millero, 1992). Because of high stability constant of REE with inorganic ligands (Luo and Byrne, 2004), a small portion of REE in solution is present as free hydrated ions (REE^{3+}). The quality and the abundance of REE inorganic complexes are dependant from the stability constant of the complexes and the relative concentration of anion ligands in solution. According to several lab experiments (Wood, 1990; Millero, 1992; Luo and Byrne, 2004), the stability constants of the trivalent REE complexes with carbonate, fluoride, phosphate and hydroxide, increase along the series from La to Lu. On the contrary, the stability constant of REE complexes with chloride have an opposite decreasing trend from La to Lu (Fig. 1.1) Moreover the chloride ligand is temperature dependant, forming weak complexes with REE at temperatures lower than 200° C and stronger complexes with the increasing temperature (Wood et al., 2003). Different behaviour is observed for REE complexes with SO_4^{2-} ligands, which constants do not change in a wide range and having an almost flat distribution and a slight MREE (Middle Rare Earth Elements) enrichment (Bulge Effect) (Millero, 1992; Johannesson et al., 1996). Carbonate complexes $[Ln(CO_3)]^+$ and $[Ln(CO_3)_2]^-$ are pH dependant, with a predominant role in near-neutral natural waters and a negligible role in strong acidic waters (Wood, 1990; Byrne et al., 2002).

Having common features as same charge and similar ionic radius (1.019 and 1.015 A, respectively), Y and Ho have similar behaviour during primary processes, with the consequence of relative Y/Ho signature in rocks close to the chondritic value (≈52, Jochum et al., 1988). During secondary process like those occurring in aqueous solutions, this signature could deviate from this reference value. During the solidification of pure silicate melt, the behaviour of these elements is

CHARAC (Charge and Radius Controlled), showing smooth normalized patterns mainly due to lanthanide contraction.

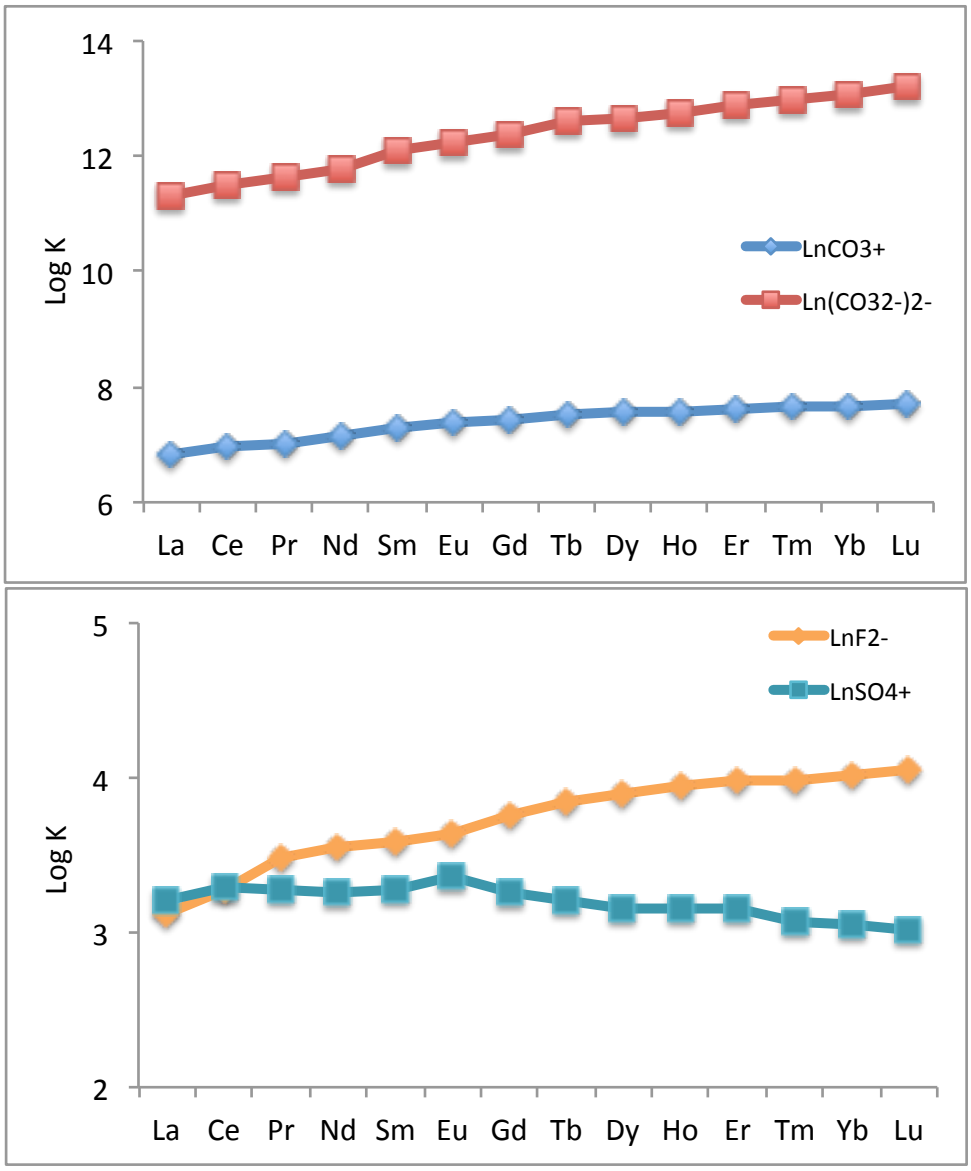

Fig. 1.1 - Stability complex for the formation of the main lanthanides complexes (Millero, 1992)

1.3 REE normalization

All natural elements follow natural abundance, characterized by Oddo-Harkins effect in which cosmic abundance of odd atomic number elements is lower than even neighbour even elements. The Oddo-Hatkins effect is perfectly evident in the Rare Earth Elements plotting the REE abundances versus the atomic number (Fig. 1.2). The common way to avoid this effect is to

normalize the REE to naturals materials and the most common used standards materials are the Post Archean Australian Shale (PAAS), the Upper Continental Crust (UCC) and the Average Chondrite. Similar distribution is shown for UCC and PAAS, characterised by a REE decreasing along the series and higher LREE/MREE and LREE/HREE ratios with respect to Average Chondrite. Different REE distribution is shown for Average Chondrite characterised by lower REE concentrations up to 2 magnitude orders (fig. 1.2).

The normalization process is used to compare REE Patterns in order to evaluate processes involving different phases generating fractionation of REE. In the last three decades, the REE dissolved in river waters are normalized most commonly to PAAS in order to evaluate chemical process in water-rock interface.

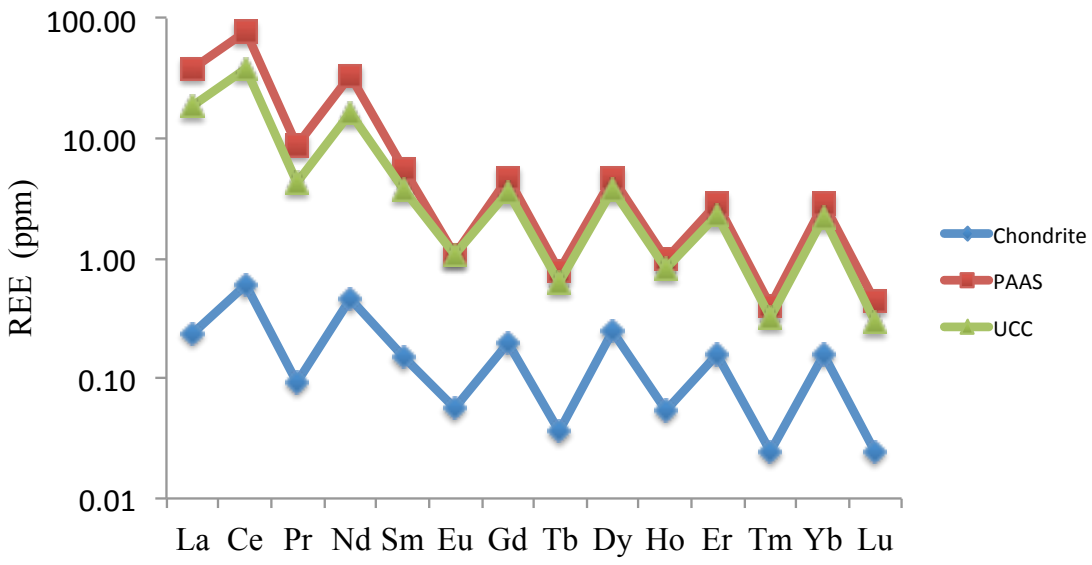

Fig. 1.2 - The distribution of Rare Earth Elements in Chondrite, PAAS (Post Archean Australian Shale) and UCC (Upper Continental Crust) expressed in ppm. Data from Taylor and McLennan, 1982; 1985; McDonough and Sun, 1995).

1.4 Role of Colloids in REE, Zr and Hf geochemistry

It is well known since the first studies (Haber, 1928), suspended particulate matter plays a dominant role in the fate of metal transport in natural water, whatever the composition organic or inorganic. Unfortunately, a clear classification of size particles is missing and studies were

conducted in an arbitrarily way, using several filtration methods. As filtration methods progressed, narrow particles size spectrum have been defined, separating any material retained at 450 and 220nm. Further technical development (ultra-centrifugation, cross-flow filtration and filed-flow fractionation) allowed extending to the colloidal realm the studies of metal-particle interactions, unveiling new aspects of metal geochemistry.

In aquatic systems colloids naturally occur, as part of a seamless continuum of elemental species stretching from fully hydrated molecules and ions all the way up to macroscopic flocs and grains (Schijf and Zoll, 2011). The aqueous geochemistry of REE, Zr and Hf is tightly coupled to particles dynamics (German et al., 1990), since they form trivalent, hard acid cations (M^{3+}) with a specific affinity for the oxygen-bearing functional groups (carboxyl, hydroxyl, phenol, etc.) that dominate organic and inorganic surfaces. Lanthanide contraction gives rise to regular and distinctively shaped patterns of stability constants and distribution coefficients for REE interactions with various ligands and sorbents. The shapes of the patterns could be diagnostic of the chemical mechanism underlying these processes. Many studies focused on YREE scavenging in estuarine zones (Sholkovitz et al., 1976; 1992; 1993; Elderfield et al., 1990), being zones of vigorous colloidal formation, explained how addition of seawater, even in slight portions, have as a consequence the precipitation of filterable particles responsible of trace metals scavenging with great efficiency. As salinity increases, major cations neutralize the distributed charge on colloids causing their collapse, along with any associated trace metals, under the sudden pressure of hydrophobic and van der Waals forces (Schijf & Zoll, 2011). As a consequence, a transition is made from riverine YREE abundance patterns to typical marine pattern with HREE enrichment, deducing that shale-like riverine REE patterns are actually a mixture of a truly dissolved HREE enriched phase with a LREE enriched colloid-bound phase. As the colloids flocculates and sinks, the HREE enriched dissolved fraction is left behind, suggesting that marine YREE patterns may in fact be largely preformed in the coastal zone on much shorter time scale, in opposition of what previously

attributed to incremental interactions between REE and settling particles over hundred of years (De Baar et al., 1985).

1.5 Zirconium and hafnium aqueous geochemistry

Zirconium and Hafnium are transition metals belonging to the IV B group of the periodic table. These elements are both tetravalent (+4) having very similar ionic radius, 0.84 Å and 0.83 Å respectively for Zr and Hf in octahedral coordination (Shannon, 1976). Their similarity is a consequence of the lanthanide contraction, conferring similar chemical-physical properties. Compared to REE, the geochemical knowledge of these elements is poor but it is well known that in natural waters their complexation is dominated by hydroxyl groups $Zr(OH)_4$, $Hf(OH)_4$, $Zr(OH)_5^-$ and $Hf(OH)_5^-$. More recent studies (Censi et al., 2014), demonstrated that $Zr(OH)_4$ and $Hf(OH)_5^-$ complexes are the dominated species in near-neutral waters, even if Zr-, Hf- complexes with fluoride and chloride ligands could be stable in hydrothermal and saline environments.

The couple of elements Zr and Hf are controlled, equally to Y and Ho, by charge and radius during the solidification of pure silicate melts, with the consequence of Zr/Hf molar ratio close the chondritic value (≈73; Jochum et al., 1986) in rock with <70% SiO_2. Different super-chondritic values have been found in aqueous solution, because Zr-Hf fractionation in solid-liquid processes is not only dependant by the ionic radius and charge (CHARAC behaviour) but it is also controlled by different metal complexation, showing a non-CHARAC behaviour (Bau, 1996).

CHAPTER 2

INVESTIGATED AREA

2.1 Caltanissetta Basin

The south-central part of Sicily is named Caltanissetta Basin, a NE-SW oriented and elongated area with an extension of about 140 km large. Caltanissetta Basin is included between the northern-most Appennino-Maghrebide range and the eastern-most Iblean plateau (fig. 2.1) and it is characterised by widespread evaporites outcrop belonging to the Gessoso-Solfifera Formation.

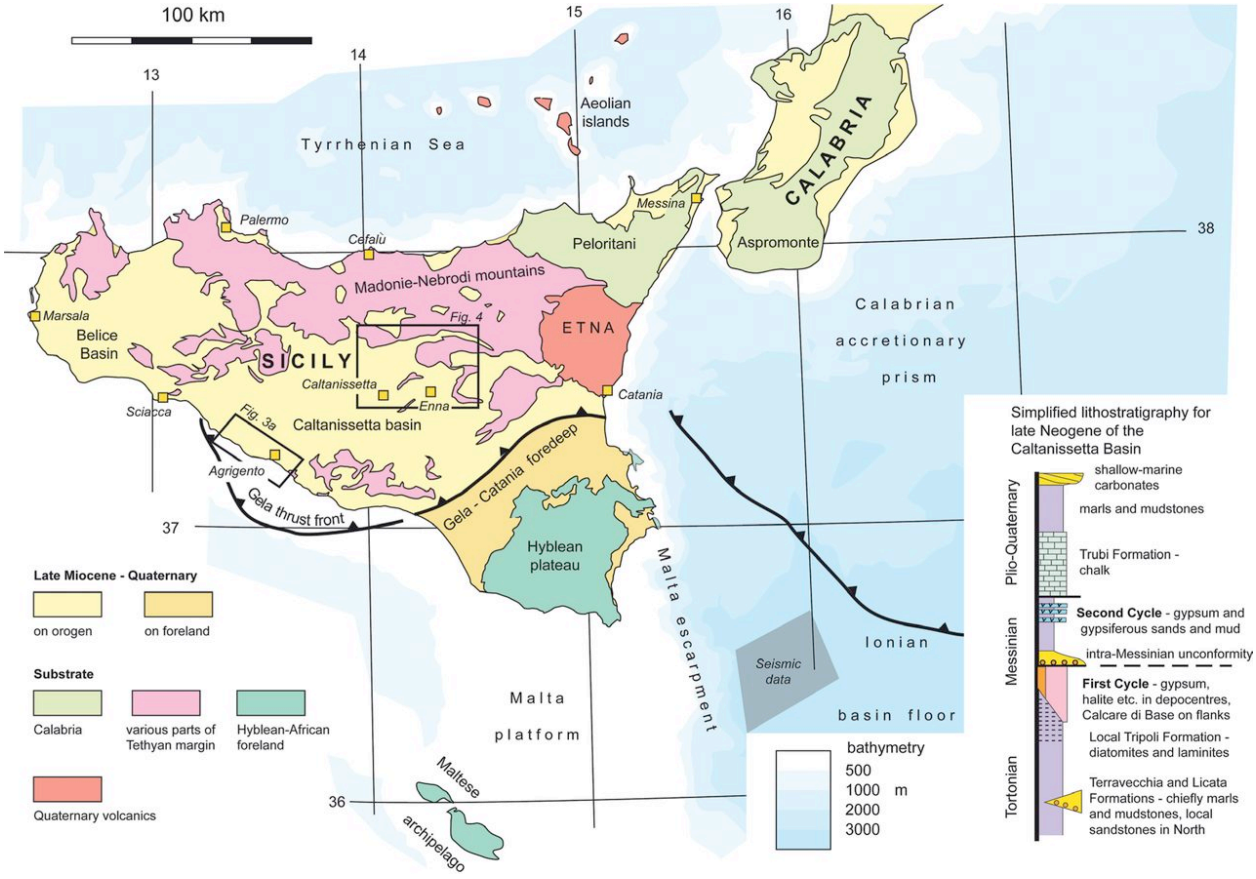

Fig. 2.1 - Regional Geological Setting of Sicily in central Mediterranean context and inset of late Neogene Quaternary stratigraphy of south-central Sicily. From Butler et al., 2014.

Sediments belonging to the Gessosso-solfifera formation were deposed during the so-called Messinian Salinity Crisis (Hsu et al., 1973) as a consequence of a progressive lack of communication between the actual Mediterranean Sea and the Atlantic Ocean.

In fig. 2.2 is shown the stratigraphic model conceived by Decima and Wezel (1973); according the authors, Gessoso-Solfifera formation can be divided in two stratigraphic units overlying diatomite sediments that represents the begin of the "Salinity Crisis":

- Lowermost Units representing the initial evaporitic deposition, consists of limestone that locally are named "Calcare di Base", followed by laminated gypsum and selenite, often embedded with gypsum marls and finally topped with salts deposits.

  The stratigraphic Unit continues with a sulphur bearing limestone, locally named "Calcare Solfifero", consisting of microcrystalline calcite, celestine, aragonite and native sulphur (Dessau et al., 1962).
- Uppermost Units are characterised by laminar, massive and clastic gypsum with marly to clay intercalations followed by a transgressive conglomerate locally named "Arenazzolo" (Manzi et al., 2009).

These two stratigraphic units are topped by the Trubi formation, consisting of foraminiferal marls, corresponding to the reopening of water communication between the evaporitic basin and the Atlantic Ocean (Cita, 1976; Rouchy et al 2001), representing the end of the Messinian salinity crisis.

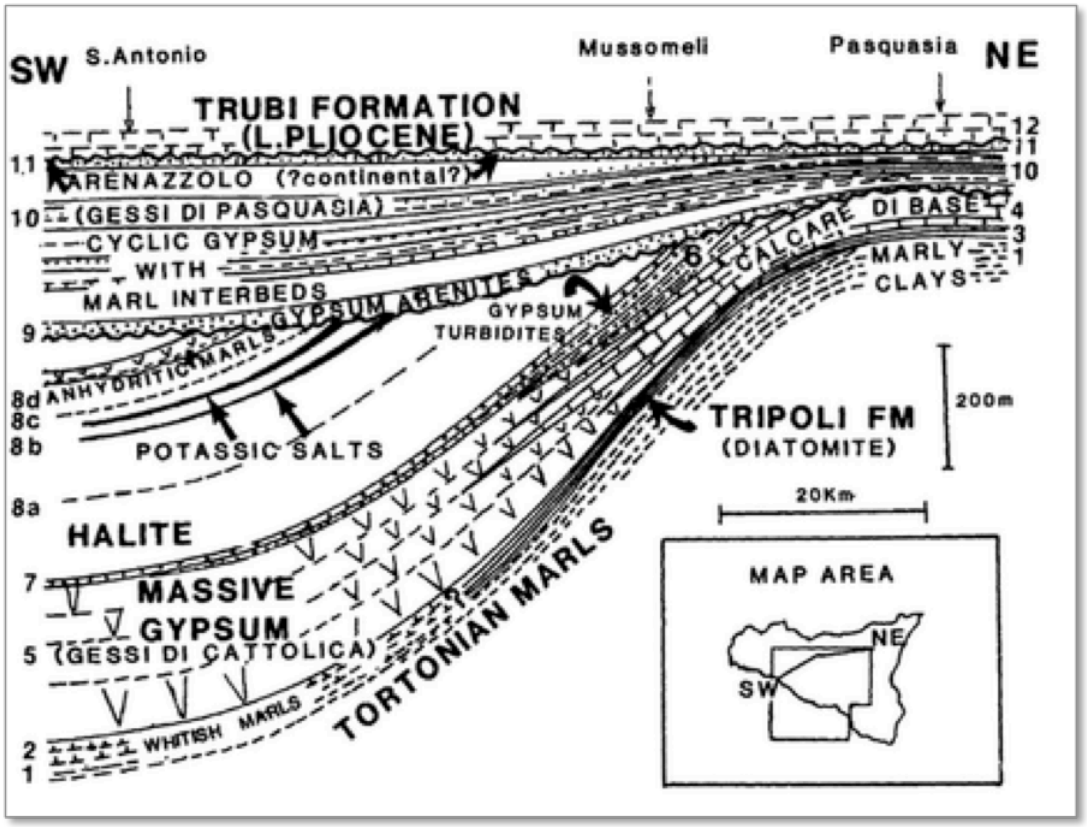

Fig. 2.2 - The stratigraphic model of Messinian Sicilian basin conceived by Decima and Wezel (1971) (From Roveri et al., 2008)

2.2 Platani drainage basin and Mining activities

Platani River catchment basin is the second widest in south-central Sicily (1777.36 km^2). It flows in NE-SW direction through the western part of the Caltanissetta basin. In particular, collecting sites of this study were mainly set in two minor drainage basins belonging to the Platani's tributaries, Gallo D'oro and Salito Rivers, having extension of 831 ands 633 km^2 respectively. These basins are set on Gessoso-Solfifera and Tortonian deposits, consisting of marls, clay marls and sandstones.

Because of sulphur and salts deposits belonging the Gessoso Solfifera Formation, the investigated area is also known for mining exploitation, now quitted. The industrial activities began between 1930 and 1938 with sulphur mine and during the exploitation of sulphur deposit, large landfills were produced close the mining area (fig. 2.3a). Detritus of "Calcare solfifero" hosting the

sulphur deposits roasted to extract sulphur formed the waste materials, mainly constituted of carbonates (calcite, aragonite) and sulphates (celestine, gypsum). Afterwards, the discovery of large kainite deposits in the 50' turned the mining activities to more promising salts exploitation. The progressively kainite mining activities produced the accumulation of a large salt landfill up to 1988, when mining activities was completely stopped. Nowadays, one of the largest saline waste deposits is set very close to minor streams and tributaries of the investigated drainage basin (fig 2.4). The weathering of these landfills by rainwater allowed to salinize the higher course of the Platani River creating the conditions for investigating the trace element fractionation among dissolved pool, suspended particles and river sediments under changing salt conditions (Censi et al., 2016).

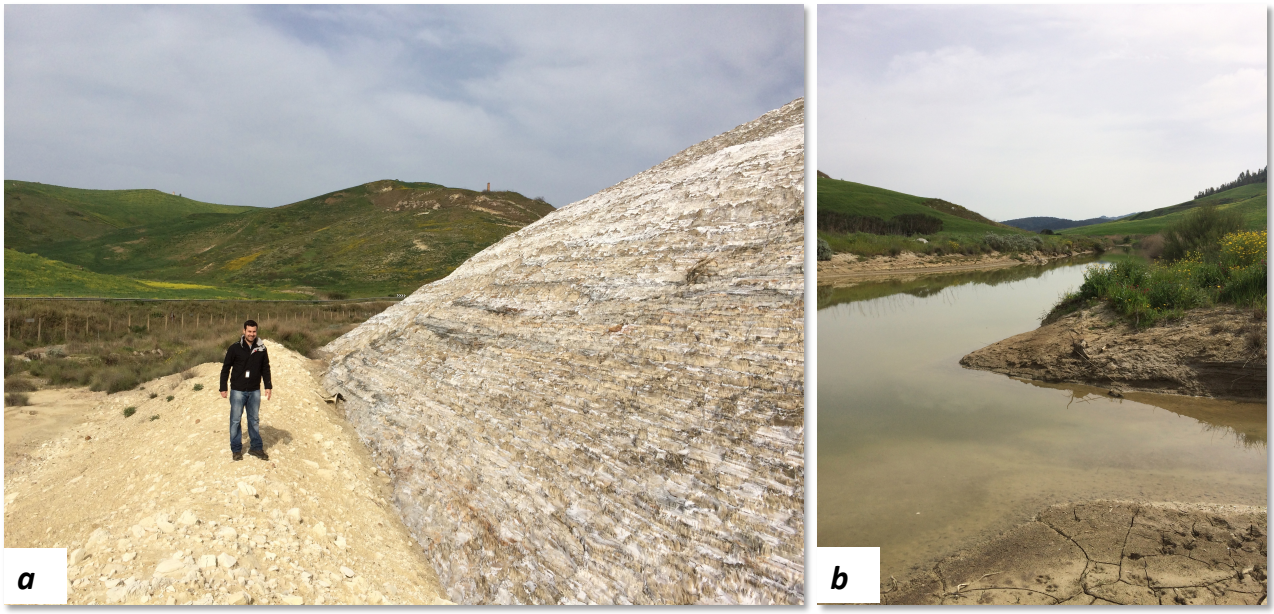

Fig. 2.3 – Photos representing the investigated area: kainite waste material (a), detail of a waters confluence.

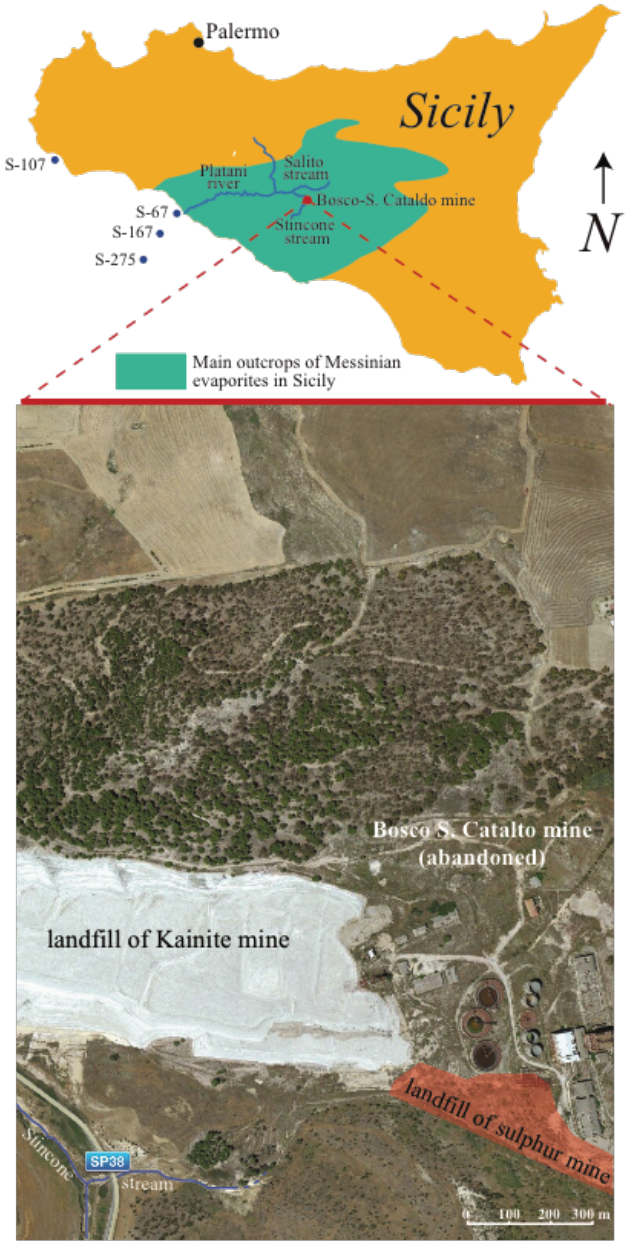

Fig. 2.4 - Caltanissetta basin and main outcrops of Messinian evaporites in Sicily. Detail of abandoned sulphur and kainite landfills (Satellite Picture from Google Earth).

CHAPTER 3

MATERIALS AND METHODS

3.1 Laboratory equipment

Sampling and lab manipulation for chemical treatment of waters and sediments were carried out using polyethylene, polypropylene or Teflon and the calibration of all volumetric equipment was verified. All chemicals reagents (HNO_3, HCl, NH_3 and H_20_2, 70%, 32-35%, 20%, 30% respectively) used during laboratory treatment were of ultrapure grade and produced by BAKER ULTRA II^{TM} (Netherlands).

Ultra-pure water (resistivity of 18.2 Ω cm) was obtained by an EASY pure II purification system (Thermo, Italy) and used for the preparation of STDs and the dilution of the samples. A calibrated E42-B balance (Gibertini, Italy) was use to weight all samples and standard.

3.2 Samples Treatments

3.2.1 Waters

Water sampling was carried out during several seasons from January 2015 and October 2016 and a total of 38 samples were collected (sampling sites are shown in fig. 3.1). Main Physical-chemical parameters like temperature, pH, Eh and electrical conductivity of waters were measured in the field with an ORION 250+meter. Eh measurement was carried out with an Eh oxytrode Pt probe (Hamilton™) using a reference standard solution buffer at 0.475±0.005 V. Accuracy of determination was ± 0.01 V for Eh, ± 0.1 for pH, ±0.1 °C for temperature and at last 1% for EC. Alkalinity was determined in the field by titration with HCl 0.1 M.

Dionex ICS 1100 chromatograph was used for major elements analysis: in particular a Dionex CS-12A column for cations, used on 50 ml of filtered and acidified (HNO_3) samples and a Dionex AS14A column used for anions on 50 ml filtered samples.

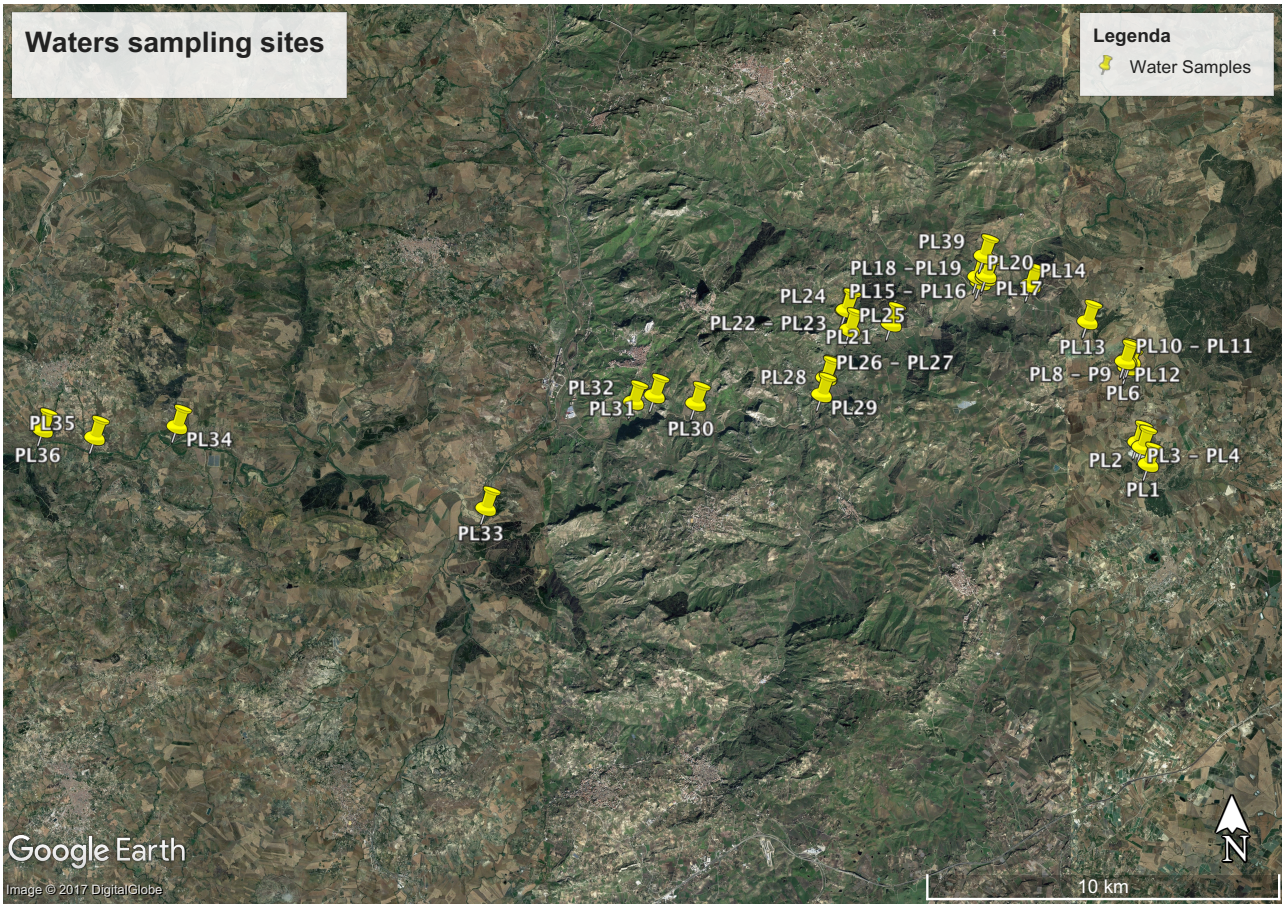

Fig. 3.1 – Location map of waters sampling sites

Thereafter, 2 more litres of water were collected at each sampling site and immediately filtered through 450 nm sterile filter membrane (CHM™ cellulose acetate filter) and then stored in previous cleaned polyethylene bottle for ultrafiltration and further lab manipulation.

Another litre of water sample was collected, filtered and acidified with 1% HNO_3 ultrapure solution to attain pH = 2 and then stored in polyethylene bottle. This is hereafter defined as dissolved fraction DF (DF < 450 nm).

The ultrafiltration procedure was carried out with a VIVAFLOW 50 ® system (10 KDa) equipped with a peristaltic pump following the procedures recommended by Sartorius Stedim Biotech GmbH,

in order to separate the colloidal fraction, defined CF (10 kDa < CF < 450 nm), from the truly dissolved fraction, defined TDF (TDF < 10 kDa) (Fig. 3.2). After the collection and relative lab manipulation, these samples were added with HNO3 ultrapure solution to attain pH = 2 and successively stored for trace elements analysis.

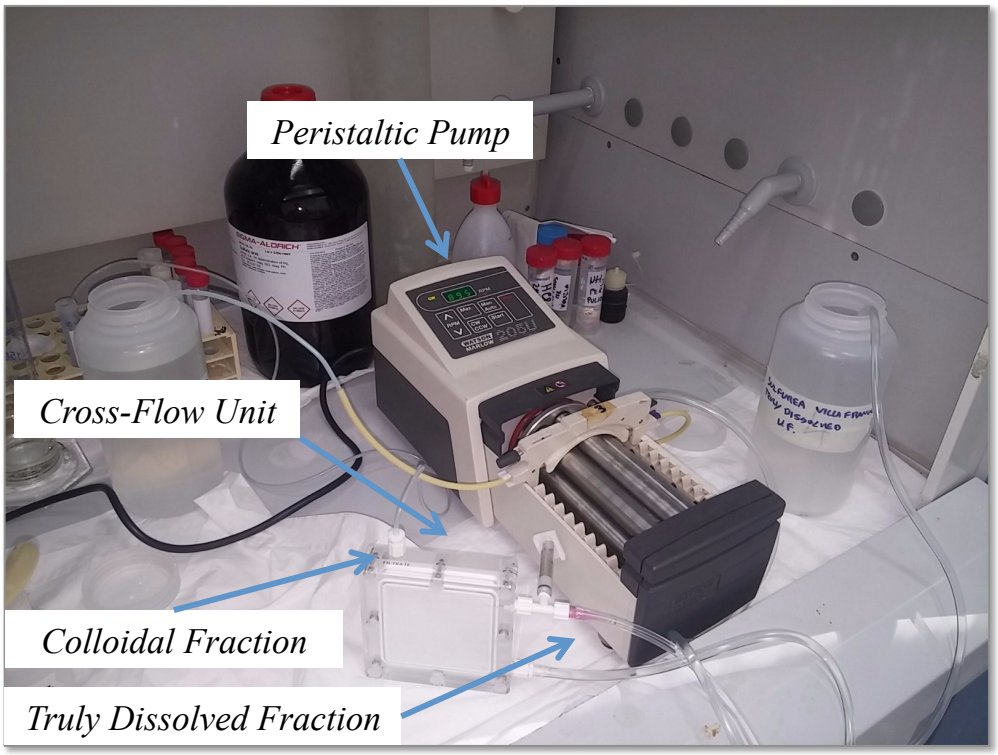

Fig. 3.2 - Lab Ultrafiltration procedure equipment: Cross-flow unit (Vivaflow 50) plugged with peristaltic pump unit. Picture from laboratories of INGV Sezione Palermo

In order to determinate the concentrations of rare earth elements, Zr and Hf, DF, CF and TDF samples were successively manipulated to selective enrichment processes of the relevant analytes, according to co-precipitation of $Fe(OH)_3$ technique reported by Raso et al (2013), (Fig. 3.2).

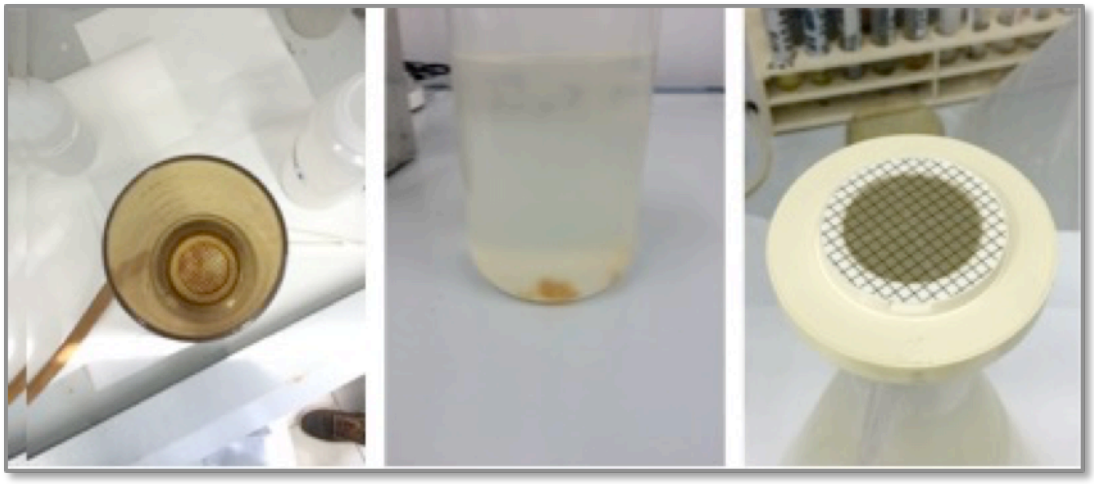

Fig. 3.3 - Samples manipulation: REE, Zr and Hf pre-concentration technique (Raso et al., 2013). Enrichment Factor (EF) ≈ 33.

The enrichment factor of this technique is about 33.3 times for each sample and the treatment was performed for a total volume of 1000 ml ± 0.005 mL. In water samples previously filtered (Millipore membranes with 450 nm porosity) and acidified (HNO_3 to attain pH = 2), were added a Fe standard solution (1000 ± 5 mg mL^{-1}), 1% $FeCl_3$ ultrapure solution (Plasma HIQU, CHEM LAB solution 1.000 µg/ml Fe^{3+}) and 25% NH4OH solution to obtain a pH ranging between 8.0 and 8.5 in order to co-precipitate lanthanides onto solid $Fe(OH)_3$. The obtained solutions were capped and stirred two hours to allow the homogenization and the further precipitation of Fe-hydroxide as a gelatinous flake. After 48h the precipitates were matured and ready for further steps: filtration, dissolution in 5 ml 6M HCl and final dilution 1:5 with ultrapure water for a final enrichment factor (EF) of 33.3 times for each sample and further analysis ICP-MS.

3.2.2 Colloids

The Colloid solutions obtained from ultrafiltration procedures were further manipulated and collected in a 20 ml Falcon vial and ultra-centrifuged (20000 rpm for 5 min). The aqueous supernatant was removed and about 500 µl of the remaining fully enriched colloids suspensions were transferred onto aluminium stub previously coated with a graphite disk. In order to evaporate

the residual water from the suspension, the stub was heated at 50 °C for minutes and used for SEM observation. Scanning electrode Microscopic (SEM) observation and EDS spectra were carried out on suspended extracted colloids (CF) collected in studied waters after ultrafiltration.

After the ultrafiltration, about 10 ml of colloidal suspension were ultra-centrifuged for 10 at 10000 rpm. The liquid fraction was gently removed by drawing and about 0.5 ml of the remained colloidal matter was placed onto a SEM pin mount. It was gently heated at about 60 °C for 30 min for evaporating residual water. Then the aluminium stub was gold coated and SEM observation and EDS analyses carried out. These were carried out using a LEO 1430 SEM (Carl Zeiss, Cambridge, UK) equipped with an EDX OXFORD INCA microanalysis system.

3.2.3 Bottom sediments

Bottom sediments of selected stream and river of Platani River basin were collected in April 2016, for a total of 7 samples and the sampling sites are shown in fig. 3.4.

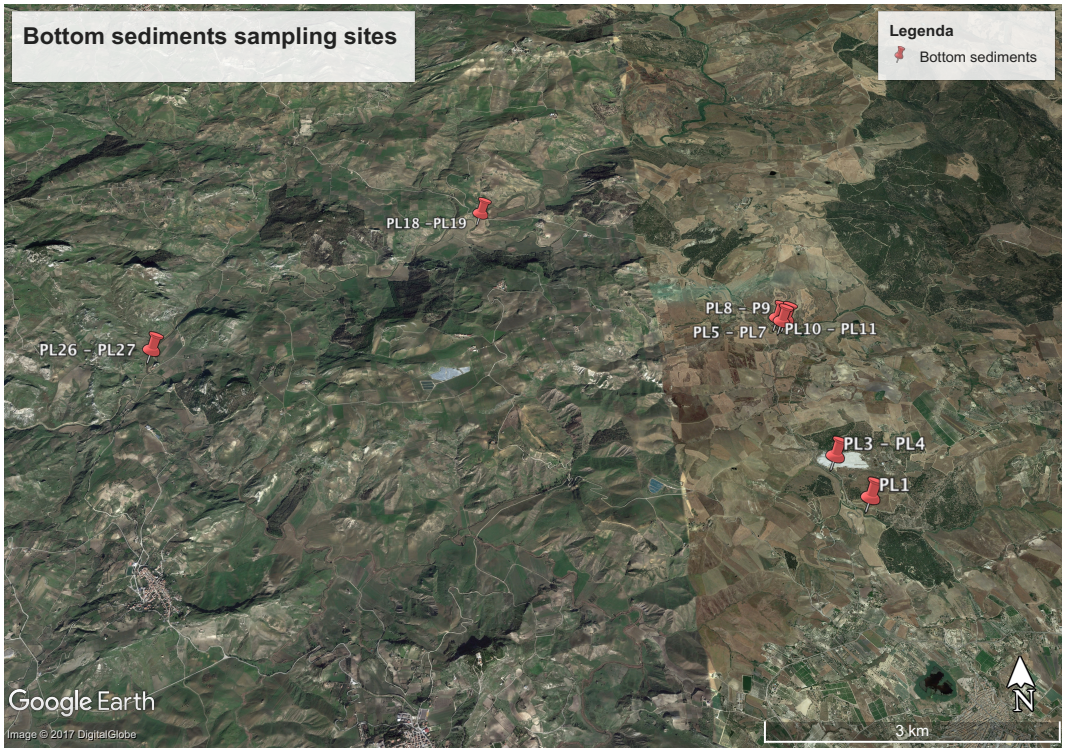

Fig. 3.4 – Location map of waters sampling sites

In order to analyse Rate Earth elements, Zr and Hf in different sediment fractions a sequential extraction was carried out, using the method proposed by Koschinsky and Halback (1995) (fig. 3.5).

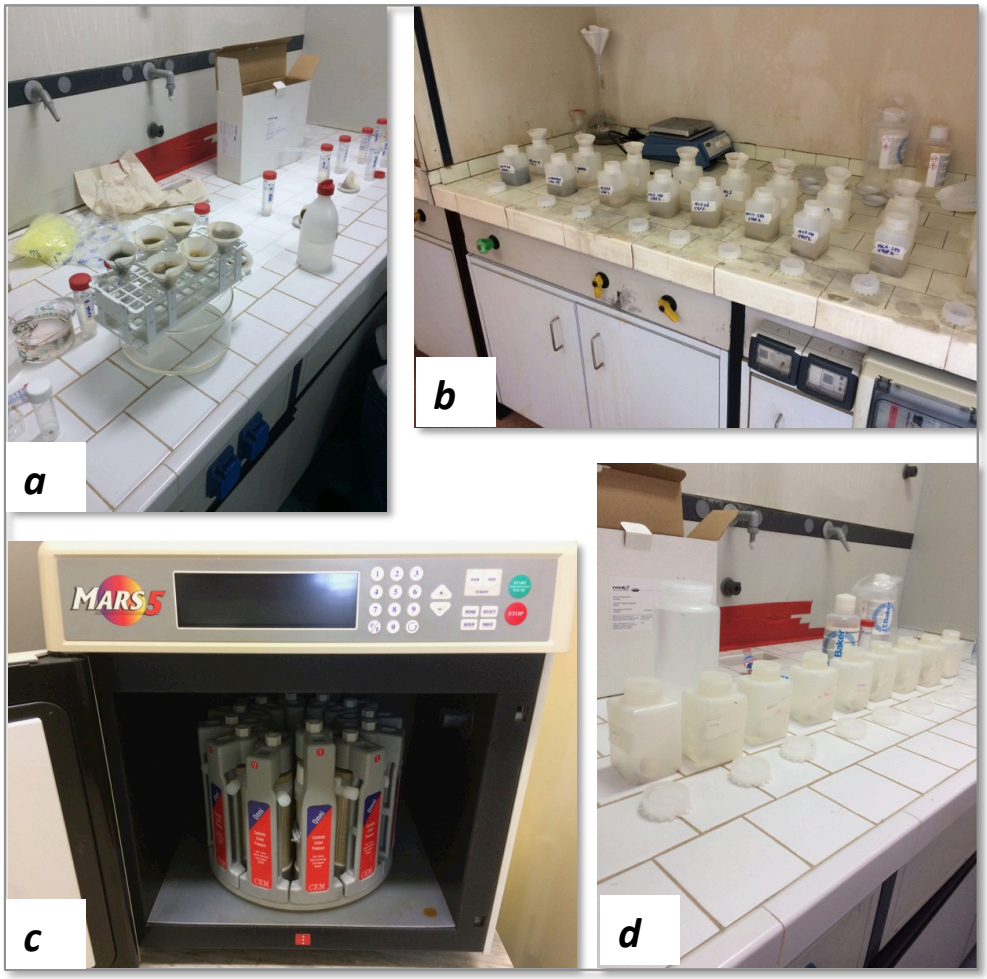

Fig. 3.5 – Lab manipulation on bottom sediments for sequential extraction (Koschinsky and Halback, 1995): a) samples filtration after 1st sequential step; b,d) 2nd and 3rd sequential step; c) 4th step final residual microwave digestion.

Sequential leaching procedures was used to analyse the concentration on four sediment fractions and the procedures were as follows:

1st Fraction: Exchangeable cations and Ca carbonates.

An aliquot of 1 g of powdered sample was added to 30 ml of an acetic acid solutions (1M), buffered with Na acetate, at room temperature for 5 hours. The solution was filtered through a 450 nm membrane filter, the residual sediment washed and the filtered solution was brought up to a final volume of 50 ml.

2nd Fraction: easily reducible fraction. 175 ml of a prepared solution of 0.1 M hydroxylamine hydrochloride (pH 2) was add to the residue of step 1 and stirred for 24 hours at 25° C. The final solution was treated as step 1 and the final volume of the filtrate was 200 ml.

3rd Fraction: moderately reducible fraction. The solid residue of step 2 was treated with 175 ml 0.2 oxalic acid, buffered with ammonia oxalate (3.5 pH) and the mixture was stirred at 25° C for 12 hours.

4th Fraction: residual-silicate fraction. The final residue of the previous steps was totally digested in Teflon bombs at 180° C for 12 hours, with a mixture solution of 3 ml of 48% HF, 3 ml of 37% HCl and 1 ml of 65% HNO3. After digestion, the solution was filtered and Millipore Water was added up to a final volume of 50 ml.

In order to check the effectiveness of the sequential leaching method, the distribution of selected major (Ti), minor (Mn, Ba, Sr) and trace elements were analysed in leachates representative of the studied sediment fractions. In the leachate of the first sediment fraction Sr, Ba and Pb, occurred. Significant Mn followed by Co, Ni and Zn contributions occurred in the leachate from the second fraction. The leachate from the third fraction mainly contained V and Th with minor contributions of Mn, Co, Ni, Cu, Sr and Ba. The largest contribution of among these studied major, minor and trace elements was measured in the solution representative of the fourth detritic fraction, apart from V, Mn, Sr and Th. Accordingly to Koschinsky and Halbach (1995), this evidence suggests that the solution from the first sediment fraction represents the release of labile bound trace elements and those coming from carbonate minerals. The solution from the second sediment fraction represents the release of trace elements from Mn-bearing phases, probably Mn-oxyhydroxides. The large geochemical coherence between V and Fe suggests that the solution from the third sediment fraction can represent the release of trace elements from Fe-bearing phases. The significant occurrence of Be, Ti, Cr, Co, Ni, Cu, Zr and others in the solution from the fourth fraction is consistent with its origin from the detritic contribution.

The obtained solutions of each procedure were suitably diluted for further ICP-Ms analysis.

3.3 Analytical methods

3.3.1 ICP-MS

Determinations of rare earth (REE), Zr, Hf and trace elements (Al, Fe, Be, Ti, Mn, Ba, Sr, Co, Ni, Cu Zn, V and Th) dissolved in water samples were carried out using an ICP-MS (Agilent 7500 cc model) at INGV (National Institute of Geophysics and Volcanology, Palermo Section) laboratories, interfaced to spectrometer software (ICP Analyst, version 5.4).

The DL of the most abundant isotopes was used, for those elements having different isotopes and the accuracy of the analysis was greater than 10% for those elements whom concentration was [X] > 5*DL and than 20% for the element with [X] <5*DL. For most of the samples, and thanks to the pre-concentration technique, the concentrations were always higher than 5*DL. The concentrations of the analytes in aqueous solution were determined by the quantitative method using the calibration solutions in a range from 0.1 to 100 μg L^{-1} for most of the elements, from 0.05 to 25 μg L^{-1} for Zr and from 2 to 2000 ng L^{-1} for REE and Hf. The weighted regression line was calculated on 10 calibrations points. All data was processed for calibration and quantitative measurements in the samples were made using ICP software (ICP Mass Hunter, version B.01.01). The standard solutions used for routine calibration of both instruments were prepared daily with CertiPUR ICP Standards Merck (Germany) and ultrapure water to 18.2 MΩ.

3.3.2 Scanning Electron Microscopy

Scanning Electron Microscopic (SEM) observations and EDS spectra were carried out on suspended extracted colloids (CF) collected in studied waters after ultrafiltration. SEM observation were carried out using a LEO 440 SEM equipped with an EDS system ISIS Link and Si (Li) PENTAFET detector that was to perform EDS spectra in the SIDERCEM S.R.L. x-ray lab (Caltanissetta, Italy).

3.4 Speciation model and REE anomalies

PHREEQC software package (version 3.0.6: Parkhurst and Appelo, 2010) was used to calculate the saturation indices (SI) and the aqueous speciation of elements. Since high salinity levels of water samples, the simulation model were carried out using the PITZER database.

Anomalies of Cerium and Europium in water fractions and sediments with respect to neighbouring elements normalized to the reference material, were calculated using the equation proposed by Alibo and Nozaki (1999):

$REE_n/REE_n^* = 2 \times (REE)_n/[(REE)_{n-1} + (REE)_{n+1}]$

Where (REE)n represent the concentration of the element choses to calculate the anomaly, while (REE)n-1 and (REE)n+1 are the previous and the subsequent element along the REE series, respectively. Anomaly of Gadolinium was calculated using the equation proposed by Moller et al., (2007): $Gd/Gd^* = Gd_n \times Ho_n^{0.5} / Tb_n^{1.}$; (1)

CHAPTER 4

HYPERSALINE WATERS

Results 4.1

4.1.1 Water characteristics

Main chemical-physical parameters, major and minor elements concentrations of the studied waters are reported in Table 4.1 (Appendix 1). Temperatures ranges between 7.5 and 31.4° C and all water samples show near-neutral pH from 7.0 to 8.6. The Total Dissolved Solids (TDS) and the Eh Values cover a wide range from 3.6 to 231.76 g l^{-1} and -0.04 to 0.20 V, respectively, while the Dissolved Organic Carbon (DOC) concentrations span between 3.92 and 13.3, mg l^{-1}, with the higher values recognised in those samples collected along the upper river path close to the Bosco Palo mine landfill.

All samples are Na and Cl dominated and in cations triangular plot (fig. 4.1) fall in proximity of and Na+K vertex; here it is possible to distinguish samples collected upstream and downstream the kainite landfill, set respectively closer to Na+K vertex or farther. Furthermore, all water samples are oversaturated with respect to carbonate minerals (Calcite and Dolomite) and evaporites (Gypsum and Anhydrite) but just for high saline samples (Tab. 4.5 Appendix 5).

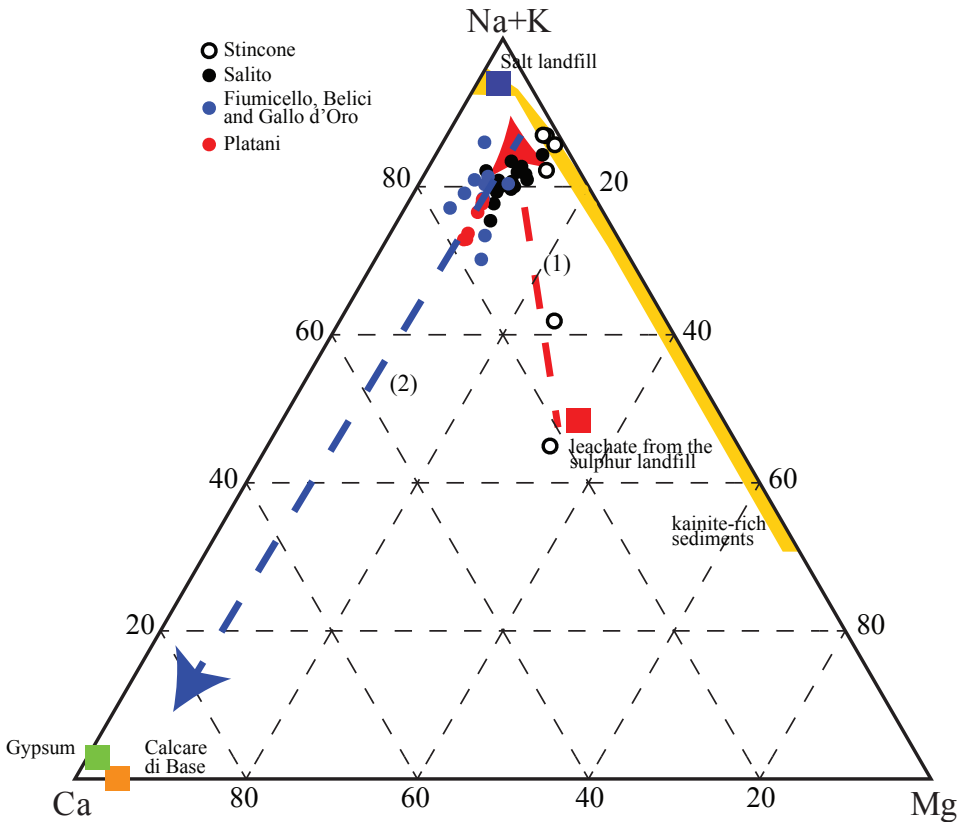

Fig. 4.1 - Triangular plot of major cations in dissolved water (DF) samples.

4.1.2 Dissolved Fraction

The REE, Zr and Hf concentrations, measured in DF are shown in tab. 4.2 (Appendix 2). Total REE concentrations range from 0.14 to 35.7 nmol l^{-1}, with higher values are found along the medium river path corresponding to Salito and Gallo D'Oro streams waters weathering large evaporites sequences. The shale-normalised REE trends can be grouped in two different patterns (Fig. 4.2): the first, hereafter defined Type-I pattern, is characterised by an ascending features determined by the progressive increase of normalised concentrations along the REE series, whereas the second, defined Type-II pattern, shows a characteristic MREE enrichment relative to LREE and HREE. Few exceptions are found in some samples with La enrichments and some evidence of Ce anomalies is observed; furthermore, several waters samples from the medium river path (Salito, Belici and Fiumicello streams) show positive Gd anomalies.

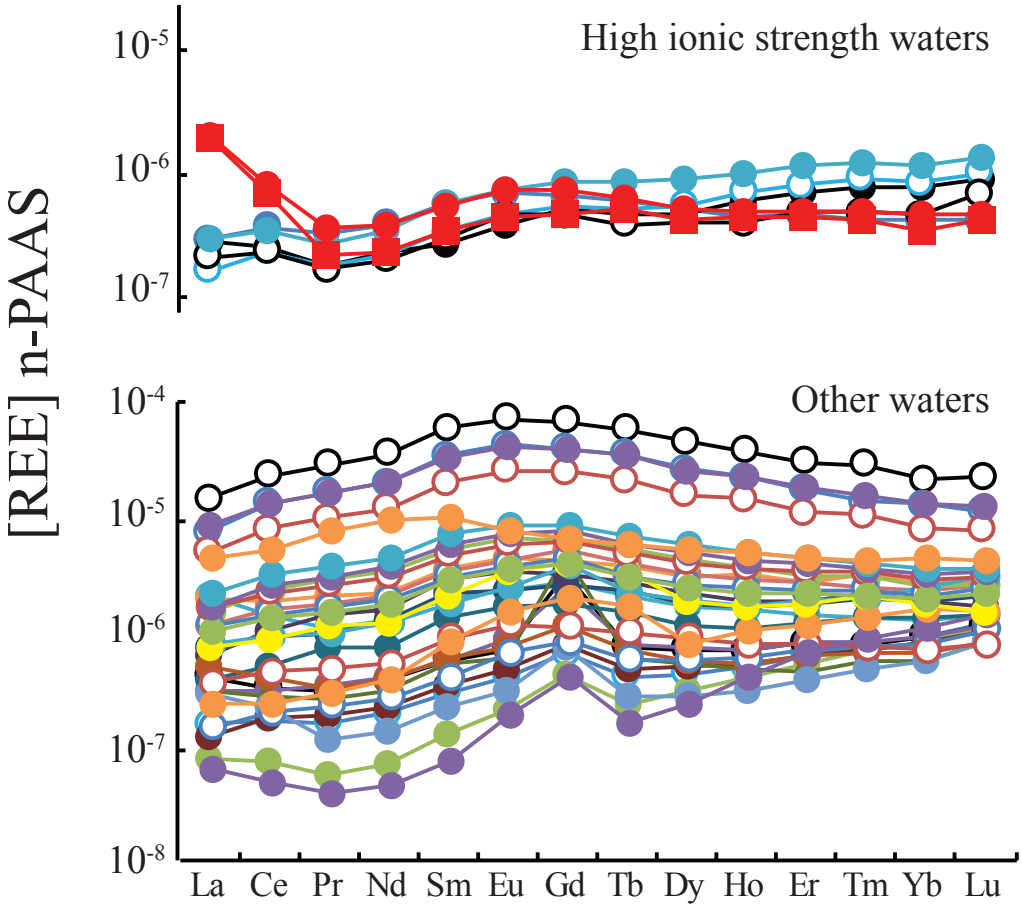

Fig. 4.2 - PAAS-Normalized REE patterns of dissolved water samples (DF).

Zr and Hf concentrations spanning in a range of values between 0.05 and 1.08 nmol l^{-1} for Zr and 0.0011 and 0.0190 nmol l^{-1} relative to Hf, (tab. 4.2, Appendix 2). Fig. 4.3 shows they are always positively correlated describing linear trends with slope close to 27 for almost all DF samples. As shown in fig. 4.3, high ionic strength samples fall along a different trend slope close to 107.

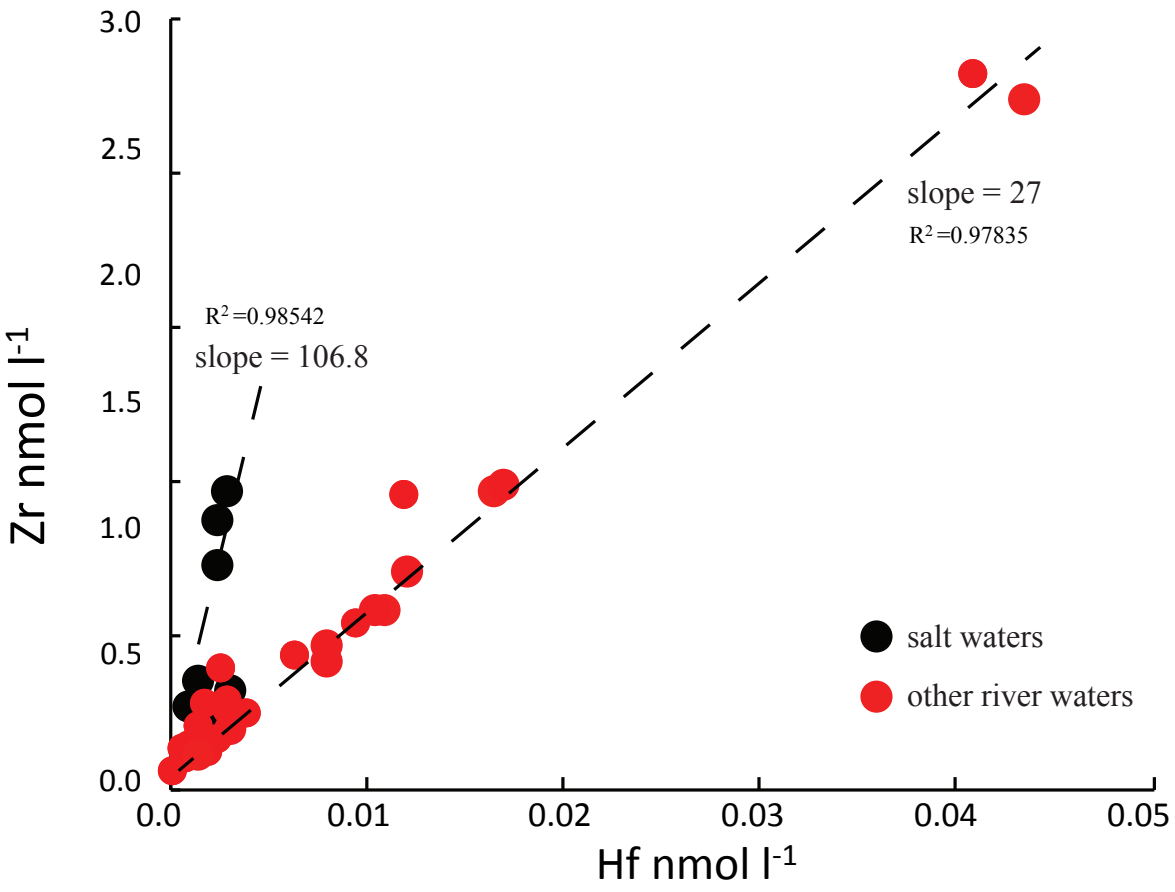

Fig. 4.3 - Zr and Hf concentrations in dissolved fraction water samples.

The Zr/Hf molar ratio values are close to chondritic signature (70.8 ± 5.6, Jochum et al., 1986) mainly in those water samples collected in the medium and lower river path corresponding to Salito, Fiumicello, Gallo d'Oro, Belici streams down to Platani River; some exceptions are represented by those samples collected along the Stincone stream where super-chondritic values Zr/Hf values are measured. On the contrary, lowest and highest Y/Ho molar ratios are found in the high river path (Stincone stream) close to the landfills of Bosco-San Cataldo mine, with values ranges from 25.1 and 90.6 and more chondritic values (51.2 ± 5, Jochum et al 1986) are found in the other sector of the investigated basin.

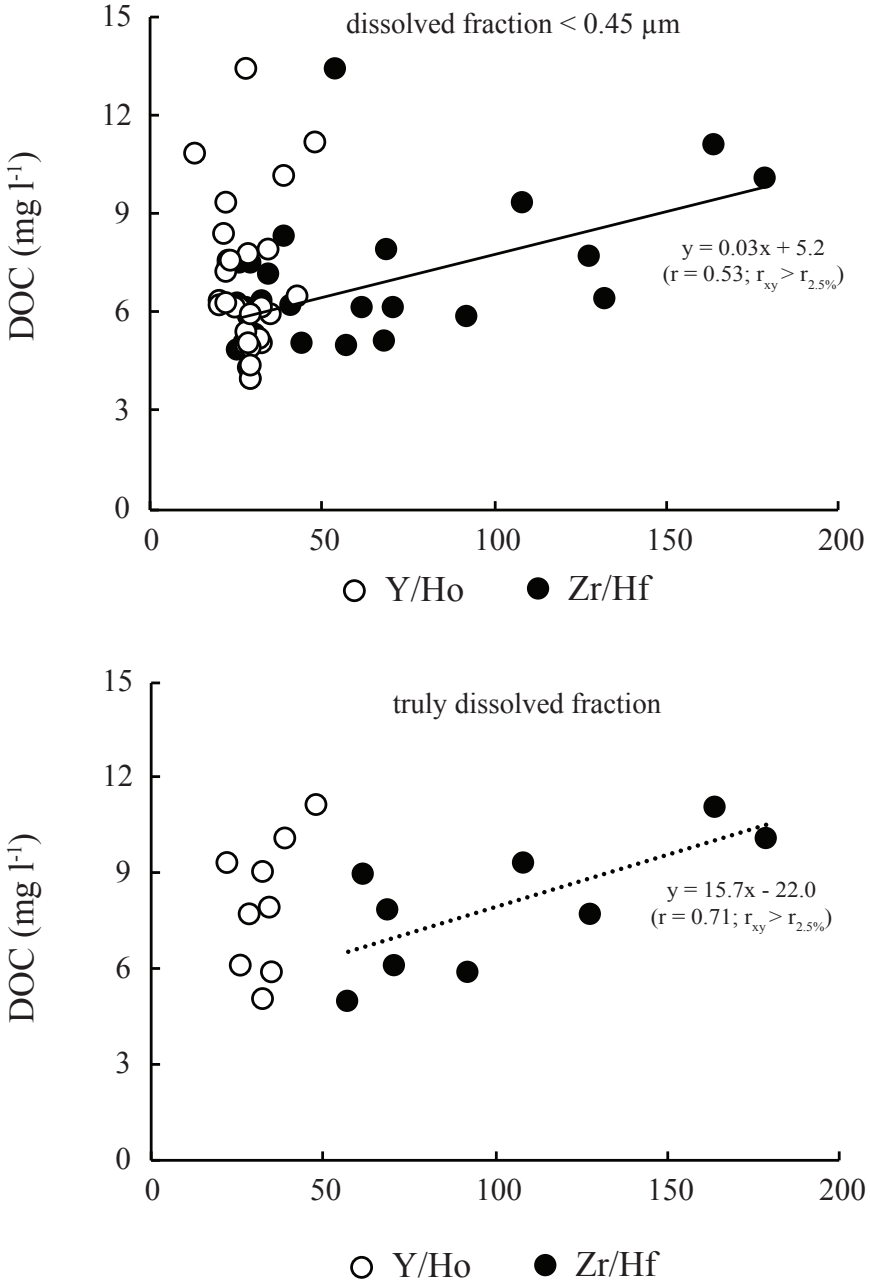

Fig. 4.4 - Correlation between Zr/Hf and Y/Ho molar ratios with DOC content

Furthermore, along the whole river path, Zr/Hf molar ratios are related to the dissolved organic content (DOC), which ranges from 3.9 and 13.4 mg l^{-1}, whereas this relation is not found for the Y/Ho ratios, as shown in fig. 4.4.

4.1.3 Colloidal fraction

The concentrations of REE, Zr and Hf measured in the CF from the investigated waters are reported in Table 4.3. REE concentrations span between 647.3 and 10464.5 pmol l^{-1} with strong enrichments in those elements from Nd to Er showing larger concentrations than La and Ce. Shale-normalised REE patterns show a general LREE depletion (Fig. 4.5), resembling to the features of type II patterns shown in REE patterns in the DF and Ce and Gd anomalies ranging respectively from 0.9 to 0.2 and from 3.5 to 1.2.

Zr and Hf concentrations spans within 1545.0 – 6686.9 pmol l^{-1} and within 82.7 and 1246.5 pmol l^{-1} ranges respectively, as a consequence relative molar ratios fall in a narrow range of sub-chondritic values from 5.4 to 28.4. At the same time, Y and Ho concentrations range between 1063.1 and 3650.4 pmol l^{-1} and from 21.7 and 338.9 pmol l^{-1} respectively with a related Y/Ho molar ratio fall between 10.8 and 98.4.

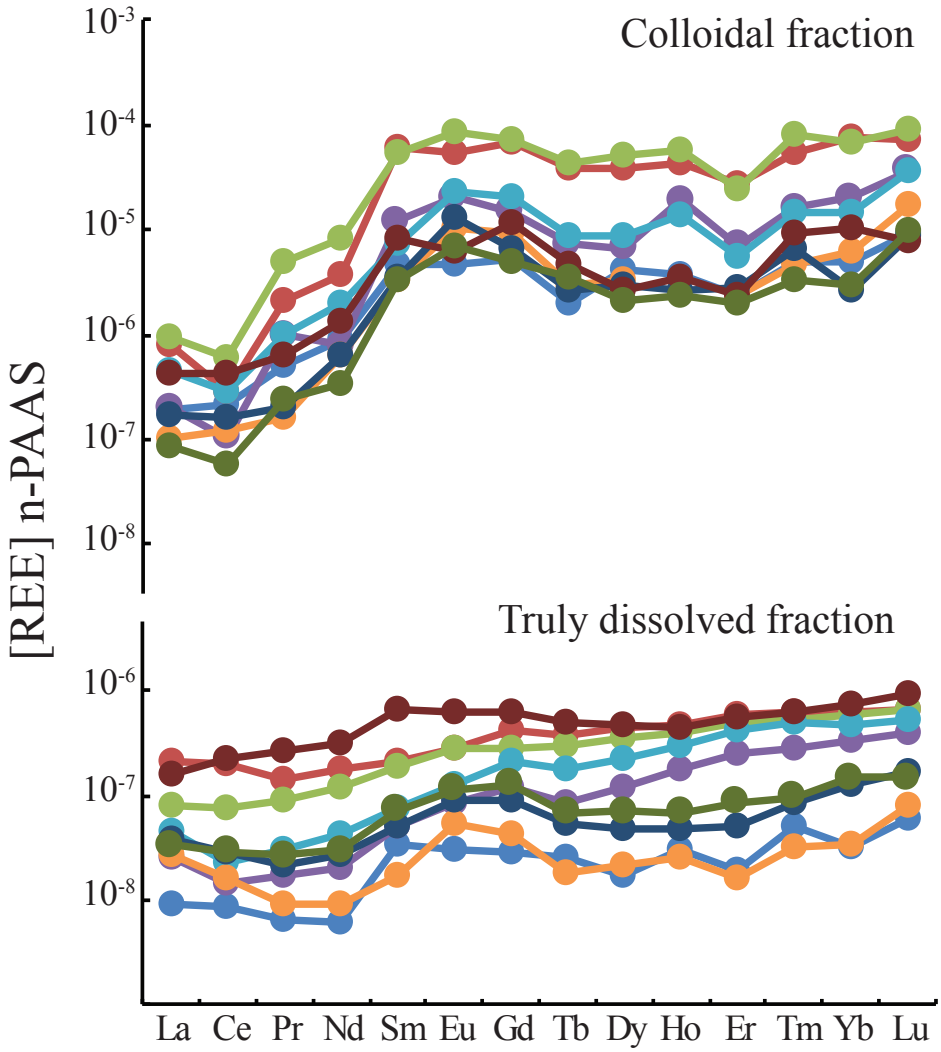

Fig. 4.5 - Comparison of PAAS-Normalized REE patterns between Colloidal Fraction (CF) and Truly Dissolved Fraction (TDF).

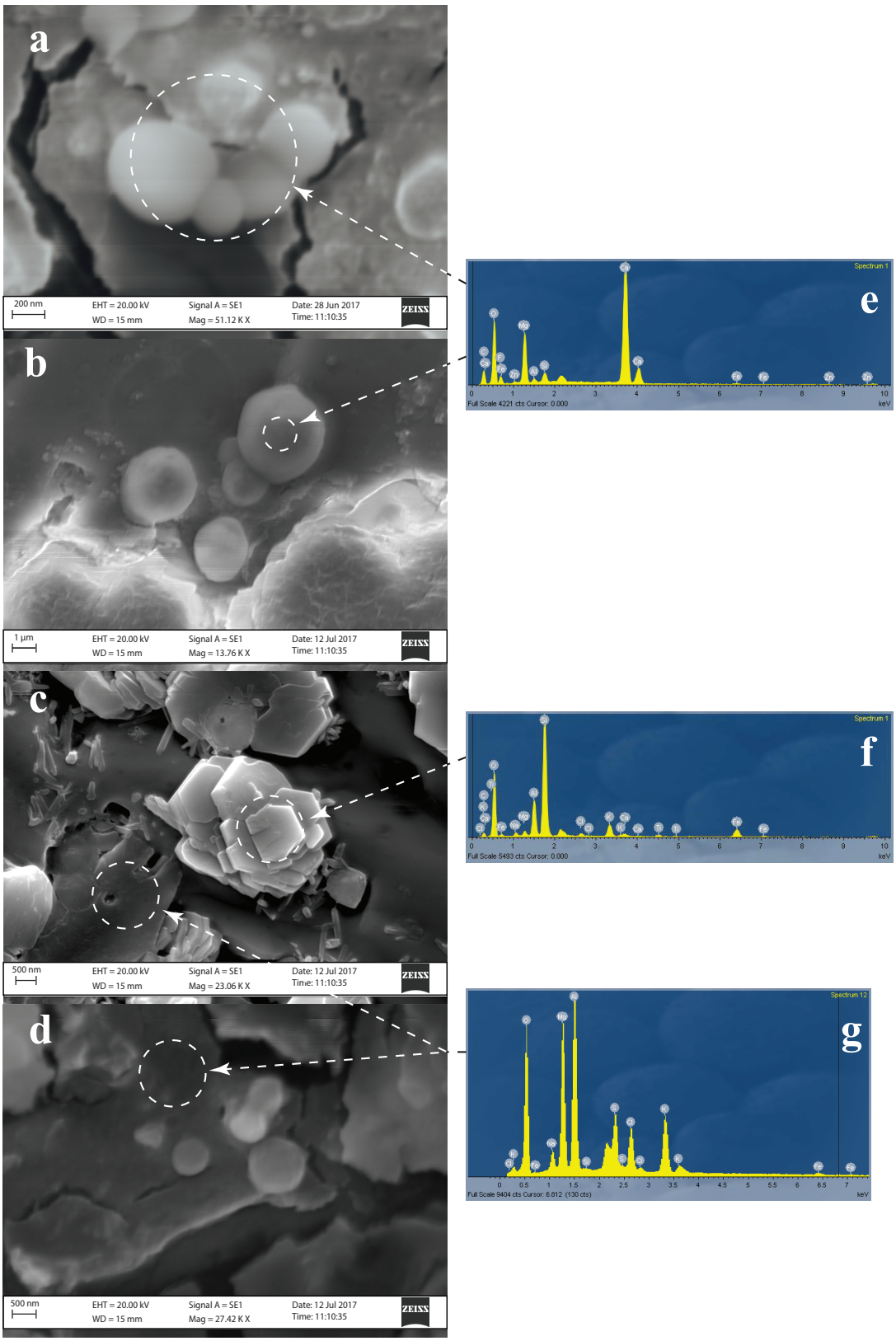

Fig. 4.6 - SEM-EDS observation of colloidal investigated fraction: a) aggregates formed by group of nanospheres. b) Some particles having up to 2 µm dimension. c-d) aggregates of clay microcrystals (100-5000nm). e-f-g) EDS spectra showing the compositions of the analysed materials.

SEM images of >10 KDa colloids extracted from selected river waters show aggregate of grouped nanospheres, having a diameter ranging from about 200 to 600 nm (fig. 4.6a), onto a fractured substratum probably as consequence of the extraction procedures; sometimes, also larger particles are shown up to about 2 μm (fig 4.6b). EDX analysis recognise the clayey nature (fig. 4.6 f-g) of aggregate microcrystal having dimension close to about 100-5000 nm sometimes scattered onto the colloidal substratum (Fig. 4.6 c-d). EDS analysis also show the Ca-, Mg-carbonate composition of nanospheres aggregates and the Al-Mg-K composition of the substratum (Fig 4.6e) The lack of any evidence of organic/biological material in extracted colloidal fraction has to be clarified as follows.

4.1.4 Truly Dissolved Fraction

The concentrations of REE, Zr and Hf measured in the TDF of the investigated water are reported in Tab 4.3. Shale normalised REE patterns shown in fig. 4.5 are different relative to those recognised in CF, since they show a progressive trends having an ascending behaviour along the REE series similar to type 1 pattern in DF water samples. Only two patterns show the above-mentioned MREE enrichment and neither Ce nor Gd anomalies are reported.

Zr and Hf concentrations are much lower than those found in the other different fractions, falling between 20.9 and 260.0 pmol l^{-1} for Zr, whereas Hf concentrations ranges between 0.2 and 1.6 pmol l^{-1}. The correspondent Zr/Hf molar ratio values fall between 84.8 and 239.2, from close to chondritic to super-chondritic values (70.8 ± 5.6, Jochum et al., 1986) with higher values measured in high saline waters. Also Y and Ho concentrations in TDF are lower than those measured in CF (6.9 and 303.4 pmol l^{-1}, 0.2 and 2.9 pmol l^{-1}, respectively) but similarly to CF and TDF, relative molar ratio values ranges from 37.2 to 105.6, with the lowest values measured in lower salinity waters.

4.2 Discussion

4.2.1 REE in aqueous pool

Shale normalised pattern in DF have two different trends and both are usually considered characteristics of a wide spectrum of geochemical processes. Type-I are attributed to the prevailing effect of dissolved REE complexation from carbonate ions or organic ligand as the stability constant of these complexes grow along the series from La to Lu (Cantrell and Byrne, 1987; Wood, 1990; Millero, 1992; Lee and Byrne, 1993; Johannesson et al., 1996; Liu and Byrne, 1997). Type II patterns in aqueous phase have been representative of several leaching process relative to phosphates (Hannigan and Sholkovitz, 2001), evaporites (Toulkeridis et al., 1998; Playa et al., 2007; Censi et al., 2017), Fe-oxyhydroxides (Bau et al., 1999) organic matter (Davranche et al., 2011), carbonates (Zhang et al., 2014) and from acid mine drainage (Grawunder et al., 2014; 2015). Type II pattern, with MREE enrichment could be also representative of the formation of REE complexes with some particular organic ligands (Tang and Johannesson, 2010; Davranche et al., 2011).

Qualitative PHREEQC model calculations on dissolved REE in DF, relative to REE speciation, partially explain the significance of Type I patterns in studied waters which features agree with the formation of carbonate complexes. The qualitative calculation of REE speciation suggests that $[REE(CO_3)]^+$ was the most stable complex in the studied river waters; this findings agrees with the observed ascending feature characteristic of Type 1 patterns (Cantrell and Byrne, 1987); Lee and Byrne, 1993; Liu and Byrne, 1988) due to increasing stability constants of $[REE(CO_3)_2]^-$ and $[REE(CO_3)]^+$ complexes (Wood, 1990; Millero, 1992). Only under higher ionic strength conditions, $[REE(CO_3)]^+$ is associated with $[REECl]^{2+}$ complexes for Ce and Pr and with $[REE(SO_4)]^+$ species for La, Nd and Sm.

Saturation index of carbonate (calcite, dolomite), Al and Fe-oxyhydroxides (Goethite, Bohemite, Gibbsite), sulphates (gypsum, anhydrite) and halides of DF water samples are shown in

appendix 5. All water samples are oversaturated with respect to carbonate minerals (Calcite and Dolomite) and evaporites (Gypsum and Anhydrite) but just for high saline samples, while any correlation between high ionic strength saturation index of Al and Fe-oxyhydroxides has been observed. As a consequence only slight correlation was found between Type-1 and Type 2 with saturation index of the considered minerals phase.

4.2.2 Gd anomaly

In the last 30 years, strong positive Gd anomaly values in dissolved phase of surface waters of anthropised countries occurred where a significant input of hospital wastewaters in river, lakes and basin, containing organic-Gd complexes, normally exploited as contrast agents in NMR imaging (Bau and Dulksi, 1996). The increasing use of this diagnostic tool in medical practices determined the exploitation of the positive Gd anomaly as geochemical tool to individuate the input of hospital wastewaters also in estuaries and coastal systems (Censi et al., 2010; Kulaksiz and Bau, 2011; 2013) Since the limited extent of observed Gd/Gd* values, not exceeding 6.5 in DF, 3.5 in CF and 2.6 in TDF, the anthropic source of Gd anomaly could be dismissed in this studied waters, because these values are far from the extent of anthropogenic" positive Gd anomalies, usually beyond 50 (Kulasisz and Bau, 2011). Furthermore, the absence of hospitals and the rural characters of the studied area make unreasonable an anthropogenic origin of the observed positive Gd anomalies. Even though it is possible that Gd anomalies could persist in absence of hospitals, caused by people who have had medical images may excrete Gd used as opacifier during x-ray analysis. Then, a more plausible explanation of these anomalies could be the same as for positive Gd anomalies observed in seawater (De Baar et al., 1995; Byrne and Kim, 1990; Kim et al., 1991), namely the larger stability of dissolved Gd complexes during solid-liquid interface processes compared with those of Eu and Tb (Erel and Stolper, 1993). Similar REE feature is observed crystallisation marine carbonates that take on the same REE distribution of parent water (Haley et

al., 2005; Tostevin et al., 2016), being the Gd distribution coefficient larger than those of the REE series during the direct calcite crystallization (Voigt et al., 2017). Positive Gd anomalies were also found in evaporitic seafloor sediments of anoxic Thetis, Kyros, Medee and Tyro basins in the Eastern Mediterranean (Censi et al., 2014) where these evaporites coexist with overlying deep-sea brines. At least, also marine biogenic carbonates show positive Gd anomaly inherited by the REE distribution in parent seawater (Haley et al., 2005)

As Shown in fig. 4.7, largest Gd/Gd* anomalies in this study are found in samples where Mg/Ca is close the unity or less, accordingly to the dissolution of Mg-calcite or dolomite. On the contrary, the dissolution of Mg-salts derived from the landfill of Bosco Palo-San Cataldo mine, does not lead to positive Gd anomalies in highly saline waters. The behaviour of Gd anomaly observed in DF also occurs in the other two investigated fractions (CF and TDF, fig. 4.7 *smaller box*), confirming that the observed positive Gd anomalies in TDF and CF are determined by the complete carbonate dissolution or by remaining carbonatic relict nanoparticles in the hetero-aggregates of colloidal pool. Thus this finding could suggest that the light positive Gd anomalies in rivers waters unaffected by anthropogenic contamination could be considered an evidence of the dissolution of primary marine limestone.

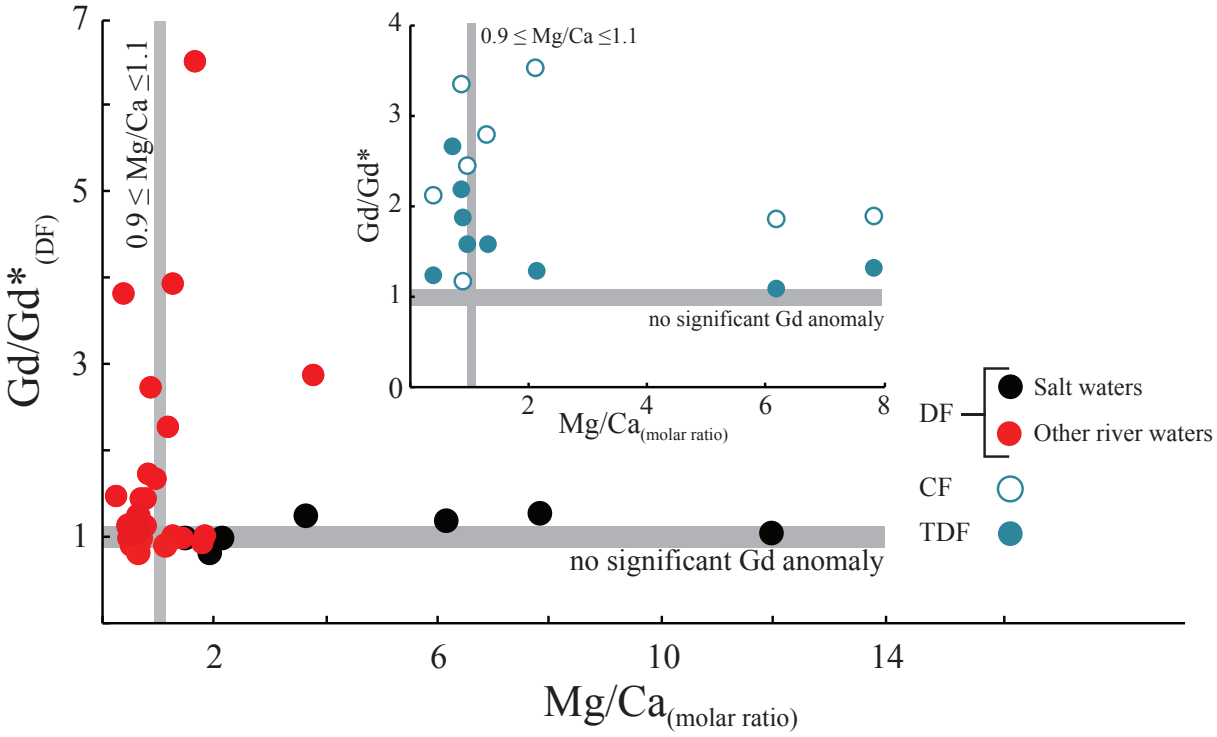

Fig. 4.7 - Relation between Gd* anomaly and Mg/Ca molar ratio in all analysed fractions. Higher Gd/Gd* values are calculated in lower salinity samples.

4.2.3 Ce anomaly

Ce anomaly is usually a specific characteristic of natural waters, considered an effect of the oxidative Ce removal from dissolved phase as precipitating insoluble CeO_2 solid (De Baar et al., 1985; Elderfield, 1988: Sholkovitz, 1995, Censi et al., 2004; 2007). Unexpectedly, shale-normalised REE patterns of 450 nm-filtered dissolved fraction do not show any significant negative Ce anomaly, but at most some samples show limited positive ones, as shown in fig. 4.8. Usually, the lack of clear Ce anomalies in natural waters could occur in organic-rich alkaline waters (Pourret et al., 2008) where oxidized Ce(IV)-species are adsorbed onto humic acids. Then, Ce removal from truly dissolved fraction is balanced by Ce uptake onto colloids and neither positive nor negative Ce anomalies are shown in the 450 nm-filtered dissolved fraction (Pourret et al., 2008). As a consequence, negative Ce anomalies would be observed only in the fraction where humic acids do not occur. In this study, humic compounds have not been detected in CF and it is proposed that their

migration in smaller size colloids occurring in the TDF. As a consequence, negative Ce anomalies should occur in CF and positive anomalies would be reported in TDF (Fig. 4.8).

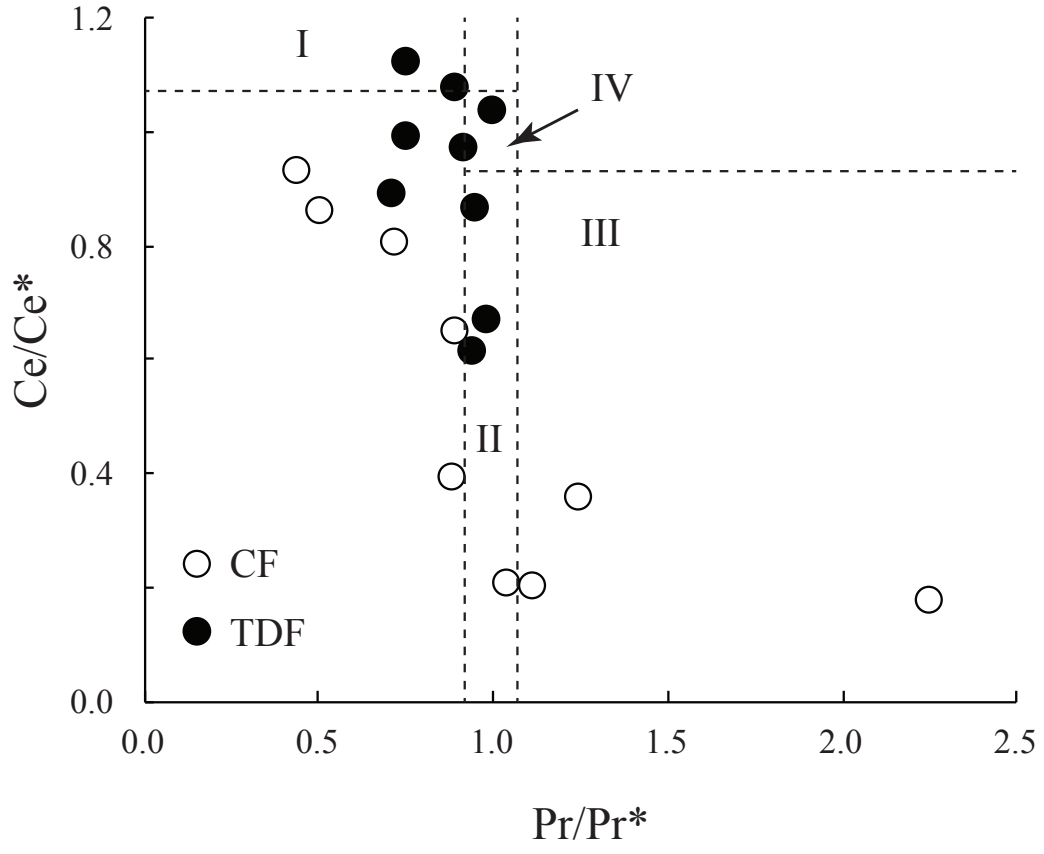

Fig. 4.8 - Ce/Ce* vs Pr/Pr* in colloidal and truly dissolved fractions.

4.2.4 Colloids Composition in studied waters

SEM observations carried out on the CF of investigated waters, indicate its inorganic nature characterised by aggregates of clay minerals and carbonate nanoparticles with Al-rich materials, probably Al-oxyhydroxides (Fig. 4.6).

These materials, having pseudohydrophylic behaviour determines the stability of nanoaggregates also at high ionic strength values (Volkova et al., 2017). Furthermore, in these waters organic

colloids have not been detected, probably due to their coagulation at high ionic strength conditions or by fractionation of humic-like fine colloidal fraction in TDF rather than in coarse CF.

4.2.5 Effect of Zr and Hf distribution between colloids and truly dissolved fraction

Sub-chondritic Zr/Hf molar ratio values measured in studied colloids suggest a greater affinity of aqueous Hf rather than dissolved Zr complexes towards the colloidal surfaces. The dissolved Zr and Hf speciation is determined, under a wide range of chemical-physical conditions, by the formation of hydroxyl-complexes (Aja et al., 1995; Veyland et al., 1998; Byrne, 2002, Qiu et al., 2009) consisting of tetramers of the oligomeric ($Zr(H_2O)_4(OH)_4$) and $Hf(H_2O)_3(OH)_5)^-$ species, respectively (Jahn et al., 2015).

Interactions of Zr and Hf aqueous complexes with available surface in natural waters usually occur according to coulombic mechanisms or by means of a surface complexation (Bau and Koschinsky, 2006). Thus, if ($Zr(H_2O)_4(OH)_4$) and $Hf(H_2O)_3(OH)_5)^-$ species interact coulombic mechanism, the preferential Hf fractionation onto colloidal surfaces requires that it is positively charged. Since the composition of the studied colloids consists of clays nanoaggregates, carbonate nanoparticles and Al-oxyhydroxides, the above mentioned hypothesis sound unreasonable, because of negatively charged surfaces from weekly acid to strong basic pH conditions (Kosmulsky, 2012). Only in the most common Gibbsite phase, Al-oxyhydroxides could be responsible of preferential Hf removal respect to the Zr in all the investigated fractions (DF, CF and TDF), due to the good dissolved ion absorbance capacity of positive surface charge, up to pH values close to 11 (Huittinen et al., 2009).

Furthermore, the larger affinity of Hf-bearing species relative to Zr complexes would agree with the hypothesis that ($Hf(H_2O)_3(OH)^-$ species may be preferentially scavenged onto colloids surfaces through a complexation mechanism where one or more OH- binding groups owing to the colloid surfaces can be involved into the inner coordination sphere of the aqueous Hf complex. In both cases the larger affinity of Hf rather than Zr towards Al-oxyhydroxides is consistent with

findings of previous studies carried out by Inguaggiato et al. (2015) and Feng (2011), reporting the larger Zr mobility relative to Hf during water-rock interaction in presence authigenic Al-oxyhydroxides. Furthermore a similar Hf preferential fractionation respect to Zr process was found by Censi et al. (2014) occurring in lithogenic nanoparticles as Ca and Mg-carbonates in colloids in evaporitic seafloor sediments of anoxic trenches of Eastern Mediterranean Sea.

Zr/Hf molar ratio values in the truly dissolved fraction span from slight sub-chondritic to extremely super-chondritic and these values are always higher than those calculated in the coexisting colloids. This evidence support the above-mentioned larger Hf affinity respect to Zr towards colloids surfaces, with the consequence of enriched Zr aqueous species in the corresponding truly dissolved fraction. Even though the paucity of data concerning Zr and Hf fractionation in natural waters, the latter evidence agrees with finding of Pokrovsky et al. (2010) in analysed natural colloid and truly dissolved fractions collected in boreal rivers.

4.2.6 Effect on REE distribution between colloidal and truly dissolved fraction

Shale-normalised REE patterns of colloidal fraction samples are characterised by significant LREE depletion (fig. 4.5), showing similarity to REE pattern shape calculated for marine dolomite. This evidence suggests that the lack of light REE element from La to Sm in colloids can be determined by their lack in dolomite where crystal-chemical reasons that do not permit the LREE substitution for Ca and/or Mg (Voigt et al. 2107). LREE depletion in CF coupled with the previous-mentioned light Gd anomalies indicates the key role played by dolomite nanoparticles in the definition of REE distribution in colloidal aggregates. As shown in fig 4.5, different features of shale–normalised patterns in TDF relative to CF are demonstrated: an ascending shape of patterns is displayed, determined by the growth of normalised REE concentrations along the series from La to Lu, in agreement to REE features for fine REE colloids in Amazon River (Rousseau et al. 2015). This evidence could suggest that TDF samples do not show Ce anomalies since humic-like colloids

take up Ce IV avoiding its sinking as CeO_2 in authigenic sediments fractions (Pourret et al., 2008; 2010; Davranche 2015; Kraemer et al., 2015). As a consequence shale-normalised patterns of CF materials show corresponding Ce/Ce* <1 values.

4.2.7 REE – Zr/Hf relationship in DF, CF and TDF

Fig. 4.9 in shows the distribution of Zr/Hf molar ratio values and REE total concentrations in DF of studied waters concurring to describe a curved array. This array could represent a cause-effect relationship between Zr-Hf behaviour and REE concentration in CF and TDF. As suggested by the hyperbolic array, the composition of <450nm dissolved pool can closely represent a mixing between two opposite starting conditions or end-members: EM-1 is identified by the largest REE concentrations coupled to the sub-chondritic Zr/Hf signature, whereas EM-2 is represented by lowest REE concentrations and super-chondritic Zr/Hf molar ratio values. In this hyperbolic trend, the highly saline waters collected downstream the landfill of Bosco-San Cataldo mine falling along the horizontal curve side, whereas the river waters showing progressively decreasing TDS values fall along the curved array.

In order to check if the array indeed represents a mixing hyperbola, in Fig. 4.9b are shown DF data plotted in a companion plot constructed between Zr/Hf molar ratio values and 1/[REE] values, where the mixing hyperbola describing the concentrations of investigated waters become a linear trend (Langmuir et al., 1978; Albarede, 1996). High ionic strength waters collected close to the Bosco S. Cataldo mine represent the only exception, falling outside the companion plot.

The arrangement of Zr/Hf and total REE concentration data in DF along the mixing hyperbola suggests that it is determined by change of reciprocal abundance of CF and TDF along the river by changing of ionic strength. In order to validate this hypothesis a mass balance calculation was carried out for CF-TDF samples according to the following equation:

$$[X]_i^{DF} = \chi^{DF}\,[X]_i^{CF} + \chi^{TDF}\,[X]_i^{TDF}; \quad (2)$$

where $[X]_I^{DF}$, $[X]_I^{CF}$ and $[X]_I^{TDF}$ are the element concentrations in DF, CF and TDF, respectively

and X^{CF} and X^{TDF} are the % fractions of these materials. The calculated values are reported in appendix 3.

Due to coagulation of colloids with the increasing salinity (Sholkovitz, 1993; 1995; Merschel et al., 2017) CF and TDF prevail at low and high ionic strength conditions, respectively.

This finding seems to be confirmed by the same hyperbolic array described plotting Zr/Hf vs REE values of CF and TDF extracted from the investigated waters, in particular CF samples fall along the vertical curve side, whereas TDF samples contribute to describe the horizontal one (Fig 4.9a). Lower REE concentrations in TDF are provided by the dissolution of salt mineral responsible of high ionic strength in waters collected close to the Bosco S. Cataldo mine; on the contrary large REE concentrations occur in CF in waters collected along the lower Platani River where ionic strength assumes lower values.

This distribution is in agreement with the larger content of colloids collected in less saline river waters (TDS <18 g l^{-1}) that progressively decrease in saline water where dissolved salts from the mine landfill lead to the coagulation of colloids (Sholkovitz, 1993; 1995). Given the above evidences in fig. 4.9a, Zr-Hf behaviour in dissolved fraction is influenced by the presence of colloids that show a larger affinity towards Hf respect to Zr, as recognised by Pokrovsky et al. (2010).

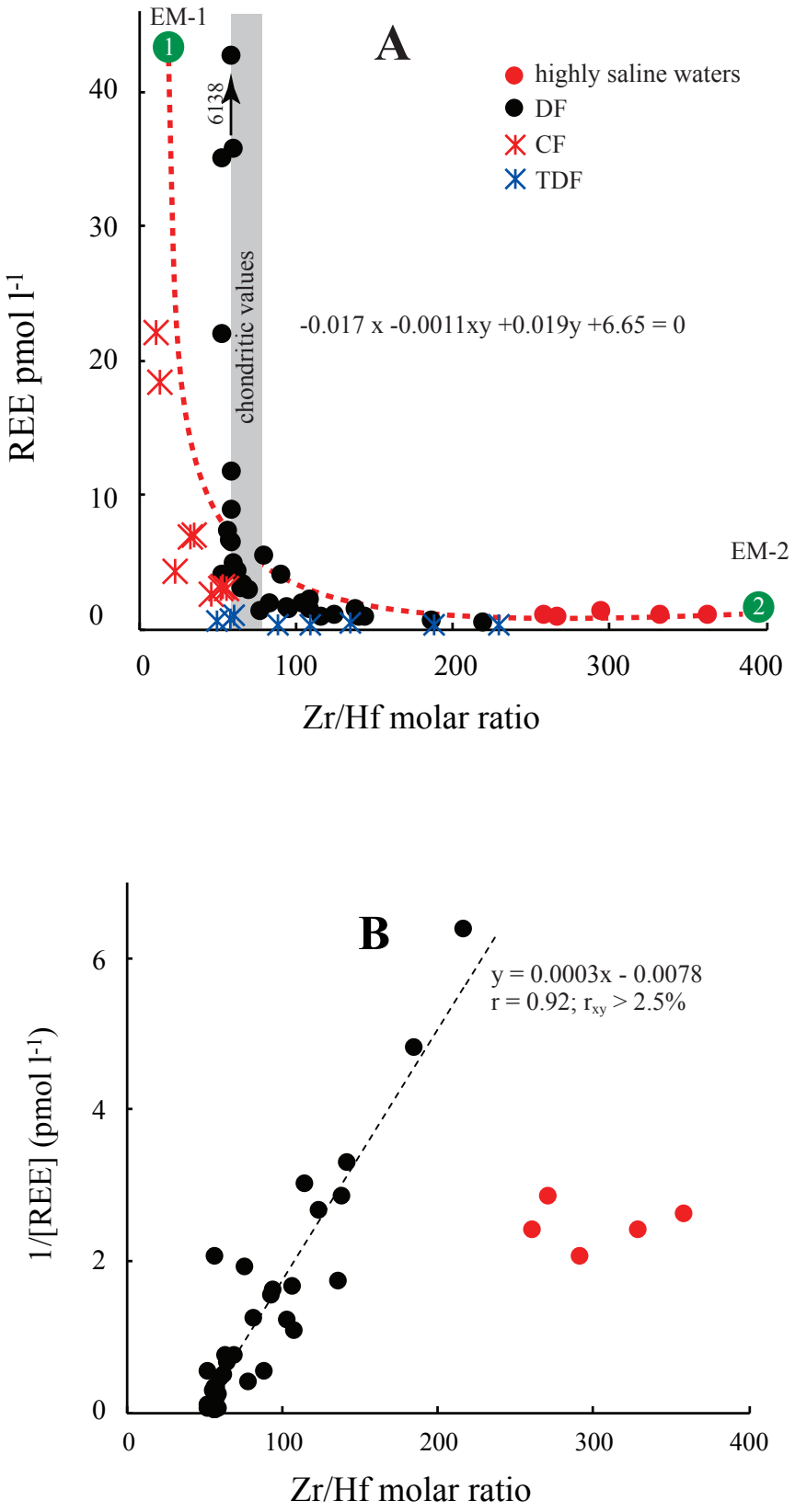

Fig. 4.9 – A) Correlation between Total REE concentrations and Zr/Hf molar ratio: mixing hyperbole B) companion plot constructed between Zr/Hf molar ratio values and 1/[REE]

CHAPTER 5

BOTTOM SEDIMENTS

5.1 Results

5.1.1 REE

REE concentrations measured in the investigated sediment fractions from the collected samples are reported in tab 4.4 (Appendix 4). In the 1st fraction (labile (Carbonate)), REE concentrations range from 21.2 and 30.6 μmol kg^{-1}; lower concentration characterised the 2nd fraction (Mn-oxyhydroxides), with measured REE concentrations spanning from 1.1 and 4.2 μmol kg^{-1}. In the 3rd fraction (Fe-oxyhydroxides) REE concentrations span between 2.6 and 17.9 μmol kg^{-1} whereas higher trace element concentrations are measured in the 4th and last fraction (silicate/residual), representing the detritic/silicate component of the total sediment composition, with total REE concentrations range between 16.5 and 469.6 μmol kg^{-1}.

The highest REE concentrations were measured in the 4th fraction ($16.5 \leq [REE] \leq 469.6$ μmol kg^{-1}), lower REE content occurred in the 1st fraction ($21.2 \leq [REE] \leq 30.6$ μmol kg^{-1}). Even lower REE content in the 2nd fraction ($2.6 \leq [REE] \leq 17.9$ μmol kg^{-1}) and in the 3rd fraction ($16.5 \leq [REE] \leq 469.6$ μmol kg^{-1}). Y/Ho molar ratio values are clustered around the chondritic range of values in the 3rd and 4th sediment fractions whereas slight super-chondritic values are found in the 1st and in 2nd fractions.

In Fig. 5.1 are shown shale-normalised REE patterns of all investigated sediment fractions. REE patterns of labile and Ca-carbonate fraction of sediments, resemble the type II pattern recognised in dissolved fraction of studied waters. There, main character is related to an almost symmetrical shape with MREE enrichment centred on Eu for each of shale-normalised trend. All samples are free from positive Ce anomalies, rather they show slight negative Ce anomaly ranging

from 0.76 to 0.86. In the 2nd sediment fraction the shape of shale-normalised patterns is almost flat with a lesser extent of MREE caused by strong positive Eu anomalies ranging from 1.40 to 3.73. MREE enrichment also occurs in 3rd sediment fraction provided by Fe-oxyhydroxide bearing minerals. Ce/Ce* values are close to 1 as a consequence no significant Ce anomalies are recognised. The shale-normalised patterns of 4th sediment fraction are almost flat in shape (similar to 2nd fraction), with some samples showing positive Eu anomalies attaining 5.32. The shale–normalised trends are symmetrical in shape centred on Eu.

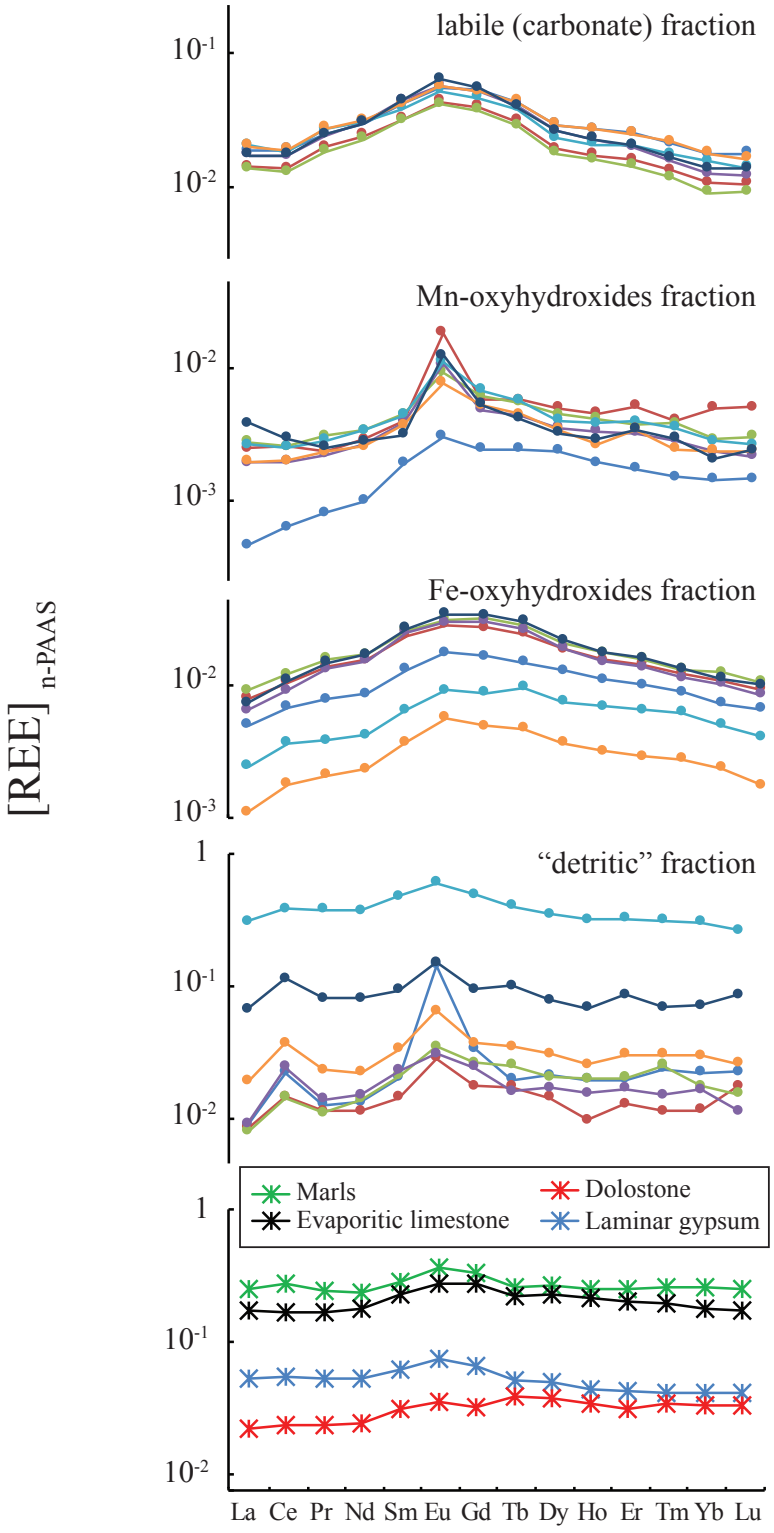

Fig. 5.1 – PAAS Normalised REE Pattern of bottom sediment fractions. For comparison are reported PAAS-Normalised patterns of Marls, Dolostone, Evaporitic limestone and Laminar Gypsum.

5.1.2 Zr and Hf

Zr and Hf concentrations of the investigated sediment fractions from the collected samples are shown in tab. 4.4 (Appendix 4). In the 1st fraction Zr and Hf concentrations range from 0.08 and 0.20 μmol kg^{-1} and from 0.002 to 0.004 μmol kg^{-1} respectively; in the 2nd one, concentration values spans from 0.02 to 0.11 μmol kg^{-1} for Zr and from 0.0001 to 0.0008 μmol kg^{-1} Hf. The 3rd is characterised by values range spanning from 1.10 to 7.02 and from 0.01 to 0.12 μmol kg^{-1} respectively for Zr and Hf. At last, larger concentrations are measured in the 4th sediment fraction, representing the detritic component of the whole chemical composition of sediment samples, showing Zr concentration between 164.5 and 1532.0 μmol kg^{-1}, whereas 2.3 and 20.1 μmol kg^{-1} for Hf.

Related Zr/Hf molar ratio values fall within the following ranges in the 1st fraction (33.4-117.7), 2nd fraction (94.4-170.9), 3rd fraction (51.1- 86.1) and the 4th fraction (71.6 – 79.9). As show in fig 5.2, Zr and Hf concentrations describe linear trends with different slopes for the analysis sediment fractions. The values of slopes range from sub-chondritic ratios in the 2nd fraction, corresponding to Mn-oxyhydroxides to super-chondritic values found in the 1st fraction corresponding to the exchangeable and carbonates sediment component. The slope of linear trend corresponding to the chondritic signature is recorded in analysis of sample from the 4th fraction corresponding to the residual and silicate sediment component.

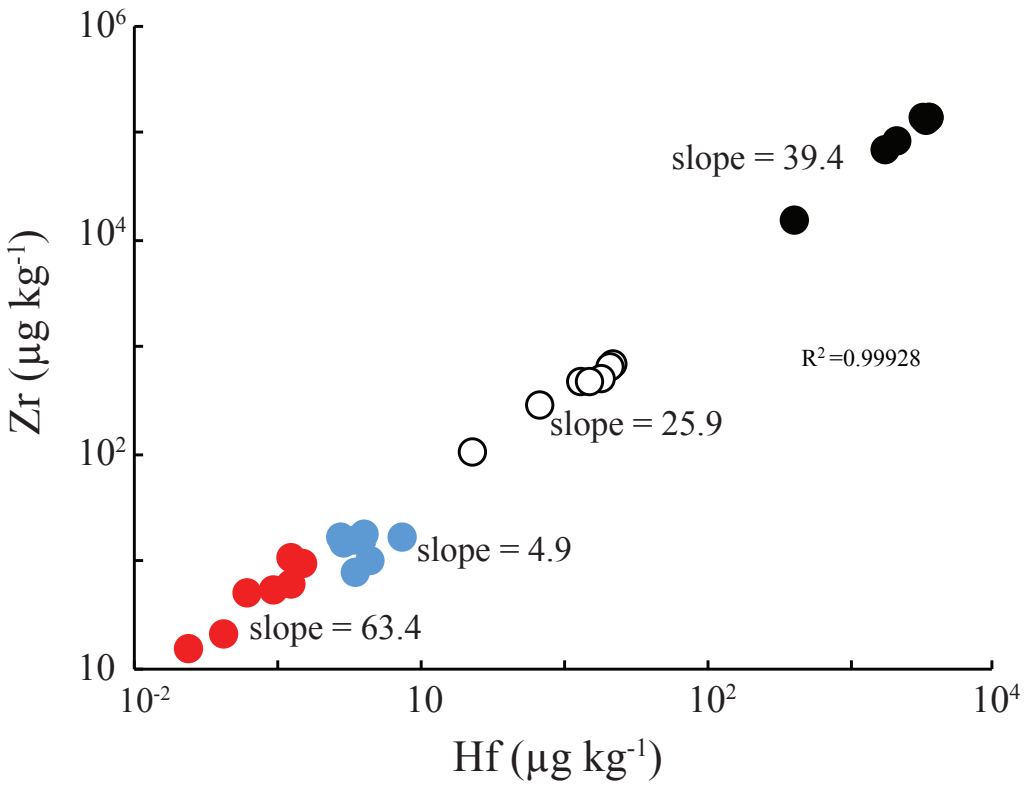

Fig. 5.2 - Zr and Hf concentrations showing a linear correlation.

5.2 Discussion

5.2.1 REE, Zr and Hf distribution in sediments

Pattern of 1st fraction is characterized by MREE enrichments as Type II pattern observed is some samples of DF and CF. Since this part of sediment total composition is representative of labile material and carbonates (Koschinsky and Halbach, 1995; Bau and Koschinsky, 2009), this evidence could suggest that the dissolution of carbonate minerals could be responsible of the distribution (Type II Pattern) of REE in river waters.

Concentrations of 2nd fraction are lower than the other considered sediment fractions and the relative shale-normalised patterns show almost flat shapes and free from Ce anomalies. On the

contrary, these patterns are characterised by positive Eu anomalies. The 2nd fraction is formed by Mn-oxyhydroxides (Koschinsky and Halbach, 1995) and since it has a negative surface charge in seawater, probably preferentially removes $[EuSO_4]^+$ positively charged species rather than $[REE(CO_3)_2]^-$ anionic complexes from aqueous pool according to a coulombic mechanism.

In terms of major elements, the chemical composition of the investigated river waters is similar to that of sea water (Na-Cl-SO_4 dominated), the formation of $[EuSO_4]^+$ species may be suggested (Millero, 1992) at high SO_4^{2-} concentration. This explanation also agrees with findings of Suya Prakash et al (2012), demonstrating the observed Eu fractionation onto Mn-oxyhydroxides relative to Sm and Gd.

In 3rd fraction, shale-normalised REE patterns are almost symmetrical in shape with a strong MREE enrichment relative to LREE and HREE without positive Ce anomalies. According to Bau et al., (2014), this distribution could be revealing the exchange equilibrium between dissolved REE species and surface REE complexes distributed onto Fe-oxyhydroxides surfaces. A Similar distribution, with MREE-enriched shale-normalised patterns was found in marine pore waters interacting with Fe-enriched source (Haley et al., 2004). Furthermore, the absence of positive Ce anomalies seems to reflect the progressive decrease in Ce/Ce* values with increasing pH, confirmed by Bau (1999) during lab experiments of REE scavenging onto Fe-oxy-hydroxides.

REE concentrations in the residual detritic/silica sediment fraction show the highest REE contents among the studied sediment fractions, testifying the origin of the studied elements in river waters from the weathering of host rocks. The relative shale-normalised REE patterns have several arrangements with the most common shape characterised by MREE enrichments, positive Ce and sometimes Eu anomalies inherited from detritic source materials. These features for the selected/considered sediment fraction, formed by aluminosilicates and crystalline oxides (Koschinsky and Halbach, 1995) agree with those typical of several river sediments (Leybourne and Johannesson, 2008; Merschel et al., 2017).

The behaviour of Zr and Hf in bottom sediments is regulated, as suggested by previous studies, by their scavenging onto available surfaces from authigenic particulate matter as colloidal fraction coagulates due to increasing ionic strength (Bau an Koschinsky, 2006; Godfrey et al., 2008). Zr/Hf values are different in all the investigated sediment fractions and if the previous mentioned process occurs also in high ionic strength waters, Zr/Hf values in CF and in the 1st, 2nd and 3rd fractions, could be similar or different: in the first case, Zr and Hf show the same affinity towards sediments surfaces, whereas in the second Zr and Hf fractionate during scavenging. In the present study, the second case occurs, as shown in fig 5.3, in which Zr/Hf values in CF are lower than those measured in authigenic sediment fractions. This evidence supports the hypothesis that the strong Hf affinity towards inorganic Al-bearing colloids and their relative resistance to coagulation at high ionic strength conditions, could determine a preferential Zr release from CF followed by Zr scavenging onto authigenic sediment fractions.

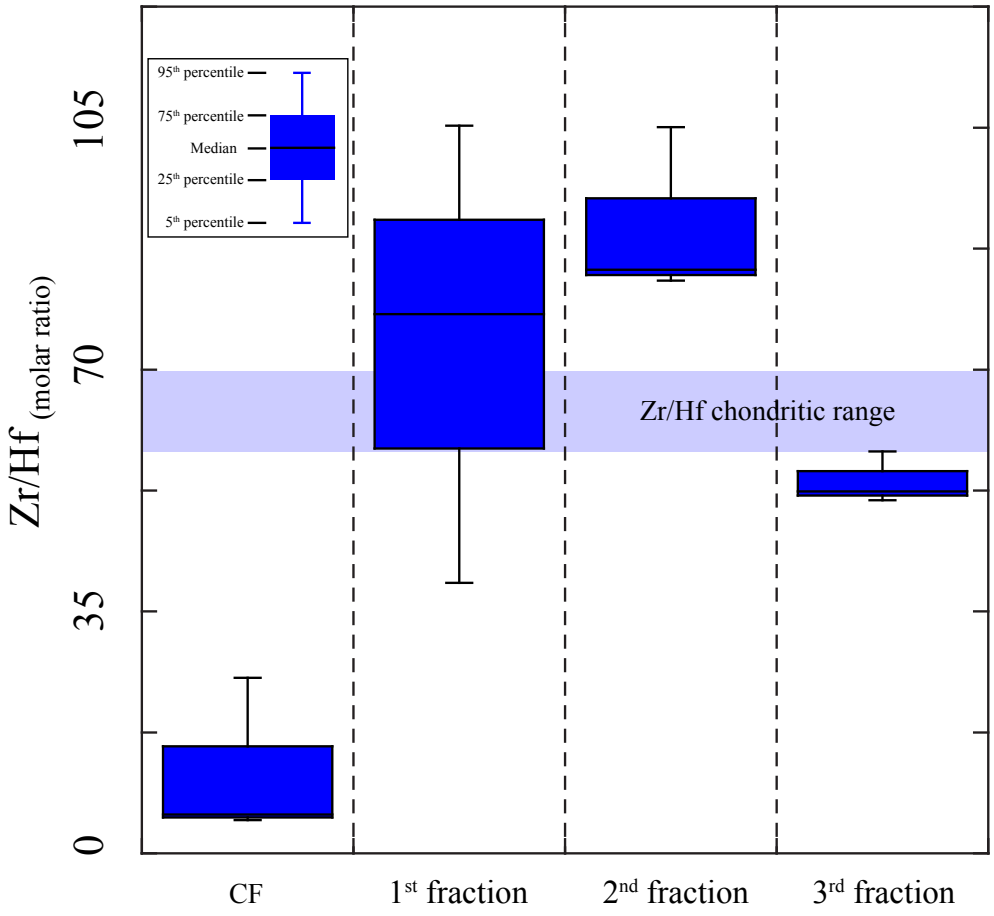

Fig. 5.3 – Comparison between Zr/Hf molar ratio in aqueous CF and 1st, 2nd and 3rd sediment fractions.

CHAPTER 6

GENERAL CONCLUSION

Achieved results of the present study represent a further step towards a more complete comprehension of the REE, Zr and Hf geochemical behaviour in hypersaline environments. This research upgrades the state of the art of the knowledge about the fractionation processes of REE and Zr and Hf in continental waters and sediments. In the specific, the behaviour of REE, Zr and Hf was studied in hypersaline waters and bottom sediments, permitting the study of these elements on different water and bottom sediments fractions in different chemical-physical conditions and a wide range of ionic strength. Particular attention has been focused on the distribution and fractionation of these elements between the colloidal and the truly dissolved fraction and how the different ionic strength may influence the stability of the colloids, considering that the latter are salinity dependent. The results indicate that the colloidal fraction dispersed in natural waters withstands also as dissolved salts exceed 200 g l^{-1}, although the amount decreases with increasing ionic strength.

This evidence is explained with the inorganic nature of nanoparticles and colloid aggregates formed by Al-oxyhydroxides carbonate nanoparticles and clay minerals. These results are consistent with the different behaviour observed in REE between organic and inorganic colloids during salt-induced coagulation. During this process, our findings suggest that Al-oxyhydroxides form a coagulation resistant fraction showing larger affinity towards Hf relative to Zr. But, even though Al-oxyhydroxides do not coagulate, the growth of ionic strength provides more Zr release in TDF rather than Hf and Zr enrichment relative to Hf is expected in river TDF accordingly to the growth of ionic strength. Under the highest ionic strength conditions observed in the studied waters, as the CF was lower in the dissolved pool, Hf preferentially interacts with carbonate surfaces in sediments. Therefore, a Zr-Hf decoupling relative to their chondritic signature could occur in rivers

or in their sediments, depending to surface/solution reactions, as colloids are formed by inorganic aggregates based on Al-oxyhydroxides.

Among the various processes that could influence the REE behaviour in natural water, the observed evidences of light positive Gd anomalies calculated in dissolved phase, colloidal and truly dissolved fraction of studied river waters and in several fraction extracted from bottom river sediments, in the view of the above, the weathering of evaporite carbonate minerals is the most reasonable to justify REE distribution.

The investigated basin, used a saline geochemical lab, is depicted by the present study as an area where the river waters show shale-normalised REE features driven by the REE speciation dominated by di-carbonate complexation and by the dissolution of outcropping carbonates determining MREE enrichment and positive Gd anomalies. Finally, the sub-chondritic Zr/Hf signature coupled with the light positive Gd anomalies found in all the analysed fractions, lead to identify the nature of colloidal hetero-aggregates as formed with the significant contribution of inorganic colloids and lithogenic nanoparticles.

Even if the hypothesis results from the present study only and has to be corroborated with Zr and Hf analyses of CF in coastal seawater, it provides another justification of the observed Zr-Hf decoupling observed in the Ocean. Therefore, this phenomenon could already start before that Zr and Hf interact with biogenic siliceous particulates in deep waters. Our results are consistent results of previous studied that ruled out the colloidal Hf pathway in TDF also under severe growth of the ionic strength.

References

Aja, S.U., Wood, S.A., and Williams Jones, A.E., 1995. The aqueous geochemistry of Zr and the solubility of some Zr-bearing minerals. Applied Geochemistry 10(6), 603-620.

Albarède, F., 1995. Introduction to Geochemical Modelling.

Alibo, D.S., and Nozaki, Y., 1999. Rare earth elements in seawater: particle association, shale normalization, and Ce oxidation. Geochim Cosmochim Acta 63, 363–372.

Bau, M., 1996. Controls on the fractionation of isovalent trace elements in magmatic and aqueous systems: Evidence from Y/Ho, Zr/Hf, and lanthanide tetrad effect. Contributions to Mineralogy and Petrology 123, 323-333.

Bau, M., and Dulski, P., 1999. Comparing yttrium and rare earth in hydrothermal fluids from the Mid-Atlantic Ridge: implications for Y and REE behaviour during near-vent mixing and for the Y/Horatio of Proterozoic Seawater. Chem. Geol. 155, 77-90.

Bau, M., and Koschinsky, A., 2006. Hafnium and neodymium isotopes in seawater and in ferromanganese crust: The “element perspective”. Earth and Planetary Science Letters 241(3), 952-961.

Bau, M., and Koschinsky, A., 2009. Oxidative scavenging of cerium on hydrous Fe oxide: Evidence from the distribution of rare earth elements and yttrium between Fe oxides and Mn oxides in hydrogenetic ferromanganese crusts. Geochemical Journal 43, 37-47.

Bau M., Schmidt, K., Koschinsky, A., Hein, J., Kuhn, and T., Usui, A., 2014. Discriminating between different genetic types of marine ferro-manganese crusts and nodules based on rare earth elements and yttrium. Chemical Geology 381, 1-9.

Butler, R.W.H., Manisclaco, R., Sturiale, G., and Grasso, M., 2014. Stratigraphic variations control deformation patterns in evaporite basins: Messinian examples, onshore and offshore Sicily (Italy). Journal of the Geological Society, 172, 113-124.

Byrne, R.H., and Kim, K.H., 1990. Rare earth element scavenging in seawater. Geochim Cosmochim Acta 54, 2645-2656.

Byrne, R.H., 2002. Inorganic speciation of dissolved elements in seawater: The influence of pH on concentration ratios. Geochemical Transactions 3, 11-16.

Cantrell, K.J., and Byrne, R.H., 1987. Temperature dependence of europium carbonate complexation. Journal of Solution Chemistry 16 (7), 555-566.

Censi P., Mazzola S., Sprovieri M., Bonanno A., Patti B., Punturo R., Spoto S.E., Saiano F. and Alonzo G. (2004). Rare Earth Elements distribution in seawater and suspended particulate of the Central Mediterranean Sea. Chem. Ecol., 20, 323–343.

Censi, P., Sprovieri, M., Saiano, F., Di Geronimo, S.I., Larocca, D., and Placenti, F. (2007). The behaviour of REEs in Thailand's Mae Klong estuary: Suggestions from the Y/Ho ratios and lanthanide tetrad effects. Estuarine, Coastal and Shelf Science 71(3-4), 569-579.

Censi, P., Incarbona, A., Oliveri, E., Bonomo, S., and Tranchida, G., 2010. Yttrium and REE signature recognized in Central Mediterranean Sea (ODP Site 963) during the MIS 6–MIS 5 transition. Paleogeography, Paleoclimatology, Paleoecology 292 (1-2) 201-210.

Censi, P., Saiano, F., Zuddas, P., Nicosia, A., Mazzola, S., and Raso, M., 2014. Authigenic phase formation and microbial activity control Zr, Hf, and rare earth element distributions in deep-sea brine sediments. Biogeosciences 11 (4), 1125-1136.

Censi, P., Sposito, F., Inguaggiato, C., Venturi, M., Censi, V., and Falcone, E.E. (2016). Weathering of evaporites: natural versus anthropogenic signature on the composition of river waters. Rendiconti Lincei 27, 29-37.

Censi, P., Inguaggiato, C, Chiavetta, S., Schembri, C., Sposito, F., Censi, V., and Zuddas, P., 2017. The behaviour of zirconium, hafnium and rare earth elements during the crystallisation of halite and other salt minerals. Chemical Geology 453, 80-91.

Cita, M.B., 1973. Mediterranean Evaporite: Paleontological arguments for a deep basin desiccation model. In: Messinian events in the Mediterranean. Kon. Ned. Ak. Wet. 206-228.

Davranche, M., Grybos, M., Gruau, G., Pédrot, M, Dia, A., and Marsac, R., 2011. Rare earth element patterns: A tool for identifying trace metal sources during wetland soil reduction. Chemical Geology 284 (1-2), 127-137.

Davranche, M., Gruau, G., Dia, A., Marsac, R., Pedrot, M., and Pourret, O., 2015. Biogeochemical Factors Affecting Rare Earth Element Distribution in Shallow Wetland Groundwater. Aquatic Geochemistry 21 (2-4), 197-215.

De Baar, H.J.W., Bacon, M.P., Brewer, P.G., and Bruland, K.W., 1985. Rare earth elements in the Pacific and Atlantic Oceans. Geochim Cosmochim Acta 49, 1943-1959.

De Carlo, E.H, and Green, W.J., 2002. Rare earth elements in the water column of lake Vanda, Mcmundo Dry Valleys, Antarctica. Geochim Cosmochim Acta 66, 1323-1333.

Decima, A., and Wezel, F.C., 1971. Osservazioni sulle evaporiti siciliane della Sicilia centro meridionale. Riv. Min. Sic., 132-139, 127-187.

Decima, A., McKenzie, J.A., and Schreiber, B.C., 1988. The origin of "evaporite" limestones: an example from the Messinian of Sicily (Italy). Journal of Sedimentary Petrology 58 (2), 256-272.

Dessau, G., Jensen, M.L., and Nakai, N., 1962. Geology and isotopic studies of Sicilian sulphur deposits. Economic Geology 57, 410-438.

Elbaz-Poulichet, F., and Dupuy, C., 1999. Behaviour of rare earth elements at the freshwater-seawater interface of two acid mine waters: The Tinto and Odiel (Andalucia, Spain). Applied Geochemistry 14 (8), 1063-1070.

Elderfield, H., and Greaves, M.J. (1982). The rare earth elements in seawater. Nature 296 (5854), 473, 214-219.

Elderfield, H., (1988). On understanding sediment geochemistry. Applied Geochemistry 3 (1), 110.

Elderfield, H., Upstillgoddard, R., and Sholkovitz, E.R., 1990. The Rare-Earth Elements in Rivers, Estuaries, and Coastal Seas and Their Significance to the Composition of Ocean Waters. Geochim Cosmochim Acta 54, 971-991.

Erel, Y., and Stolper, E.M., 1993. Modeling of rare-earth element partitioning between particles and solution in aquatic environments. Geochim Cosmochim Acta 57, 513-518.

Feng, J.L. (2011). Trace elements in ferromanganese concretions, gibbsite spots, and the surrounding terra rossa overlying dolomite: Their mobilization, redistribution and fractionation. Journal of Geochemical Exploration 108 (1), 99-111.

Firdaus, M.L., Minami, T., Norisuye, K., and Sohrin, Y., 2011. Strong elemental fractionation of Zr-Hf and Nb-Ta across the Pacific Ocean. Nat. Geosci. 4, 227-230.

German, C.R., Klinkhammer, G.P., Edmond, J.M., Mura, A., and Elderlfield, H., 1990. Hyfrothermal scavenging of rare-earth elements in the ocean. Nature 345, 516-518.

Godfrey, L.V., White, W.M., and Salters, V.J.M., 1996. Dissolved zirconium and hafnium distributions across a shelf break in the northeastern Atlantic Ocean. Geochim. Cosmochim. Acta 60, 3995-4006.

Godfrey, L. V., and Field, M. P., 2008. Estuarine distributions of Zr, Hf, and Ag in the Hudson River and the implications for their continental and anthropogenic sources to seawater. Geochem. Geophys. Geosyst. 9, 359-370.

Goldstein, S. J., and Jacobsen, S. B., 1988. Rare earth elements in river waters. Earth Planet. Sci. Lett. 89, 35-47.

Gonzalez-Alvarez, I., and Kerrich, R., 2009. REE and HFSE mobility due to protracted flow of basinal brines in the mesoproterozoic Belt-Purcell Supergroup, Laurentia. Precambrian Research 177 (3-4), 291-307.

Grawunder, A., Merten, D., and Büchel. G., 2014. Origin of middle rare earth element enrichment in acid drainage-impacted areas. Environ Sci Pollut Res Int 21 (11), 6812-6823.

Grawunder, A., Lonschinski, M., Merten, D., and Büchel. G., 2015. Rare earth elements as a tool for studying the formation of cemented layers in an area affected by acid mine drainage. Applied Geochemistry 54, 100-110.

Haber, F., and Gesellsch. Erdk. Z., (Suppl. 3) (1928) 3.

Haley, B.A., Klinkhammer, G.P., and Mix, A.C., 2005. Revisiting the rare earth elements in foraminiferal tests. Earth and Planetary Science letters 239 (1-2), 79-97.

Hannigan, R.E., and Sholkovitz, E.R., 2001. The development of middle rare earth element enrichments in freshwaters: weathering of phosphates minerals. Chemical Geology 175 (3-4), 495-508.

Huittinen, N., Rabung, T., Lützenkirchen, J., Mitchell, S.C., Bickmore, B.R., and Lehto, J., (2009). Sorption of Cm(III) and Gd(III) onto gibbsite, α-Al(OH)<inf>3</inf>: A batch and TRLFS study. Journal of Colloid and Interface Science 332 (1), 158-164.

Hsu, K.J., and Ryan, W.B.F., 1973. Comments on "The crustal structure of the Balearic Sea" – in light of deep-sea drilling in the Mediterranean. Tectonophysics, 20 (1-4), 303-306.

Inguaggiato, C., Censi, P., Zuddas, P., Londono, J.M., Chacon, Z., and Alzate, D., 2015. Geochemistry of REE, Zr and Hf in a wide range of pH and water composition: The Nevado del Ruiz volcano-hydrothermal system (Colombia). Chemical Geology 417, 125-133.

Jahn, S., Dubrail, J., and and Wilke, M., 2015. Complexation of Zr and Hf monomers in supercritical aqueous solutions: Insights from *ab initio* molecular dynamics simulations. Chemical Geology 418, 30-39.

Jochum K. P., Seufert H. M., Spettel B., and Palme H., 1986. The solar-system abundances of Nb, Ta, and Y, and the relative abundances of refractory lithophile elements in differentiated planetary bodies. Geochim Cosmochim Acta 50, 1173-1183.

Johannesson, K.H., Berry Lyons, W., Yelken, M.A., Gaudette, H.E., and Stetzenbach, K.J., 1996. Geochemistry or rare-earth elements in hypersaline and diluite acidic natural terrestrial waters: Complexation behavior and middle rare-earth element enrichments. Chemical Geology 133 (1-4), 125-144.

Johannesson, K.H., Palmore, C.D., Fackrell, J., Prouty, N.G., Swarzenski, P.W., Chevis, D.A., Telfeyan, K., White, C.D., and Burdige, D.J., 2107. Rare earth element behavior during groundwater-seawater mixing along the Kona Coast of Hawaii. Geochem Cosmochim Acta 198, 229-258.

Kerrich, R., and Xie, Q., 2002. Compositional recycling structure of an Archean super-plume: Nb-Th-U-LREE systematics of Archean komatiites and Basalts revisited. Contributions to Mineralogy and Petrology 142 (4), 476-484.

Kim, K.H., and Byrne, R.H., Lee, J.H., 1991. Gadolinium behaviour in seawater: a molecular basis for gadolinium anomalies. Marine Chemistry 36(1), 107-120.

Kosmulski, M., 2012. IEP as a parameter characterizing the pH-dependent surface charging of materials other than metal oxides. Advances in Colloid and Interface Science 171-172, 77-86.

Kosmulski, M., and Rosenholm, J.B., 2002. The specific adsorption of sodium cations on less common metal oxides at high ionic strengths. Journal of Colloid and Interface Science 248 (1), 30-32.

Koschinsky, A., and Halbach, P., 1995. Sequential leaching of marine ferromanganese precipitates: Genetic implications. Geochim Cosmochim Acta 59, 5113-5132.

Koschinsky, A., and Hein, J.R., 2003. Uptake of elements from seawater by ferromanganese crusts: solid-phase associations and seawater speciation. Mar. Geol. 198, 331–351.

Kraemer, D., Kopf, S., Bau, M., 2015. Oxidative mobilization of §cerium and uranium and enhanced release of "immobile" high field strength elements from igneous rocks in the presence of the biogenic siderophore desferrioxamine B. Geochim Cosmochim Acta 165, 263-279.

Kulaksiz, S., and Bau, M., 2011. Anthropogenic gadolinium as a microcontaminant in tap water used as drinking water in urban areas and megacities. Applied Geochemistry 26 (11), 1877-1885.

Kulaksiz, S., and Bau, M., 2013. Anthropogenic dissolved and colloid/nanoparticle-bound samarium, lanthanium and gadolinium in the Rhine River and the impeding destruction of the natural rare earth element distribution in rivers. Earth and Planetary Science Letters 362, 43-50.

Langmuir, C.H., Vocke Jr, R.D., Hanson, G.N., and Hart, S.R., 1978. A general mixing equation with applications to Icelandic basalts. Earth and Planetary Science Letters 37 (3), 380-392.

Lawerence, M.G., Greig, A., Collerson, K.D., and Kamber, B.S., 2006. Rare Earth Element and YttriumVariability in South East Queensland Waterways. Aquatic Geochemistry 12(1) 39-72.

Lee, J.H., and Byrne, R.H., 1993. Complexation of trivalent rare earth elements (Ce, Eu, Gd, Tb, Yb) by carbonate ions. Geochim Cosmochim Acta 57, 295-302.

Leybourne M. I. and Johannesson K.H., 2008. T Rare earth elements (REE) and yttrium in stream waters, stream sediments, and Fe–Mn oxyhydroxides: Fractionation, speciation, and controls over REE + Y patterns in the surface environment. Geochim Cosmochim Acta, 72, 5962–5983.

Liu, X., and Byrne R.H., 1997. Rare earth and yttrium phosphate solubilities in aqueous solution. Geochim Cosmochim Acta 8, 1635-1633.

Luo, Y.R., and Byrne, R.H., 2004. Carbonate complexation of yttrium and the rare earth elements in natural waters. Geochim Cosmochim Acta 68, 691-699.

Manzi, V., Lugli, S., Roveri, M., and Schreiber, C., 2009. New facies model for the Upeer Gypsum of Sicily (Italy): chronological and paleoenvironmental constrains for the Messinian salinity crisis in the Mediterranean. Sedimentology, 56, 1937-1960.

McDonough W. F., and Sun S. S., 1995. The composition of the earth. Chem. Geol. 120, 223–253.

McKelvey B. A., and Orians K. J., 1993. Dissolved zirconium in the North Pacific Ocean. Geochim Cosmochim Acta 57, 3801-3805.

Merschel, G., Bau, M., Schmidt, K., Münker, C., and Dantas, E.L., 2017. Hafnium and neodymium isotopes and Rey distribution in the truly dissolved, nanoparticulate/colloidal and suspended loads of rivers in the Amzon Basin, Brazil. Geochem Cosmochim 213, 383-399.

Millero, F.J., 1992. Stability-Constants for the Formation of Rare-Earth Inorganic Complexes as a Function of Ionic-Strength. Geochim Cosmochim Acta 56, 3123-3132.

Moller P., Rosenthal, E., Geyer, S., Guttman, J., Dulski, P., Rybakov, M., Zilberbrand, M., Jahnke, C., and Flexer, A., 2007. Hydrochemical processes in the lower Jordan valley and in the Dead Sea area. Chemical Geology 239 (1-2), 27-49.

Nugent, L.J., 1970. Theory of the tetrad effect in the lanthanide(III) and actinide(III) series. Journal of Inorganic Nuclear Chemistry, 32, 3485– 3491.

Parkhurst, D.L., and Appelo, C.A.J., 2010. User's Guide to PHREEQC (Version 2.17.5)-A Computer program for Speciation, Batch- Reaction, One-Dimensional Transport and Inverse Geochemical Calculations. Available at: http://www.brr.cr.usgs.gov/projects/ GWC_coupled/phreeqc/index.html.

Playa, E., Cendòn, D.I., Travé, A., Chivas, A.R., and Garcia, A., 2007. Non-marine evaporites with both inherited marine and continental signatures: The Gulf of Carpentaria, Australia, at ≈ 70 ka. Sedimentary Geology 201 (3-4), 267-285.

Pokrovsky, O.S., Viers, J., Shirokova, L.S., Shevchenko, V.P., Filipov, A.S., and Dupré, B., 2010. Dissolved, suspended, and colloidal fluxes of organic carbon, major and trace elements in the Severnaya Dvina River and its tributary. Chemical Geology 273 (1-2), 136-149.

Pourret, O., Davranche, M., Gruau, G., and Dia, A., 2008. New insights into cerium anomalies in organic-rich alkaline waters. Chemical Geology 251 (1-4), 120-127.

Pourret, O., Gruau, G., Dia, A., Davranche, M., and Molenat, J., 2010. Colloidal Control on the Distribution of Rare Earth Elements in Shallow Groundwaters. Aquatic Geochemistry 16 (1), 31-59.

Qiu, L., Guzonas, D.A., and Webb, D.G., 2009. Zirconium dioxide solubility in high temperature aqueous solutions. Journal of Solution Chemistry 38 (7), 857-867.

Raso, M., Censi, P., and Saiano, F., 2013. Simultaneous determinations of zirconium, hafnium, yttrium and lanthanides in seawater according to a co-precipitation technique onto iron-hydroxide. Talanta 116, 1085-1090.

Rouchy, J.M., Orszag-Speber, F., Rouchy, and Panayides, J.-M., 2001. Paleoenvironmental changes at the Messinian-Plocene boundary in the Eastern Mediterranean (southern Cyprus basins): Significance of the Messinian Lago-Mare. Sedimentary Geology 145 (1-2), 93-117.

Rousseau, T.C.C., Sonke, J.E., Chmeleff, J., Van Beek, P., Souhaut, M., Boaventura, G., et al. (2015). Rapid neodymium release to marine waters from lithogenic sediments in the Amazon estuary. Nature Communications 6.

Shannon, R.D., 1976. Revised effective ionic radii and systematic studies of interatomic distances in halides and chalcogenides. Acta Cryst A32: 751–767.

Schijf, J., and Zoll, A.M., 2011. When dissolved is not truly dissolved – The importance of colloids in studies of metal sorpion on organic matter. Journal of Colloid and Interface Science 36, 137-147.

Sholkovitz, E.R., 1976. Flocculation of dissolved organic and inorganic matter during the mixing of river and seawater. Geochim Cosmochim Acta 40, 831-845.

Sholkovitz, E.R, 1992. Chemical evolution of rare earth elements: fractionation between colloidal and solution phases of filtered river water. Earth and Planetary Science Letters 114 (1), 77-84.

Sholkovitz, E.R, 1993. The geochemistry of rare earth elements in the Amazon River estuary. Geochem Cosmochim 57 (10), 2181-2190.

Sholkovitz, E.R, 1995. The aquatic chemistry of rare earth elements in rivers and estuaries. Aqautic Geochemistry 1 (1), 1-34.

Surya Prakash, L., Ray, D., Paropkari, A.L., Mudholkar, A.V., Satyanarayanan, M., Sreenivas B., et al., 2012. Distribution of REEs and yttrium among mojor geochemical phases of marine Fe-Mn-oxides: Comparative study between hydrogenous and hydrothermal deposits. Chemical Geology (312-313), 127-137.

Tang, J., and Johannesson, K.H., 2006. Control on the geochemistry of rare earth elements along a groundwater flow path in the Carrizo Sand aquifer, Texas, USA. Chemical Geology 225 (1-2), 156-171.

Tang, J., and Johannesson, K.H., 2010. Ligand extraction of rare earth elements from aquifer sediments: Implication for rare earth complexation with organic matter in natural waters. Geochim Cosmochim Acta 74, 6690-6705.

Taylor, S.R., and McLennan, S.M., 1995. The geochemical evolution of the continental crust. Reviews of Geophysics 33 (2), 241-265.

Tostevin R., Shields, G.A., Tarbuck, G.M., He, T., Clarkson, M.O., and Wood, R.A., 2016. Effective use of cerium anomalies as a redox proxy in carbonate-dominated marine settings. Chemical Geology 438, 146-162.

Toulkeridis, T., Podwojewski, P., and Còauer, N., 1998. Tracing the source of gypsum in New Caledonia soils by REE contents and S-Sr isotopic composition. Chemical Geology 145 (1-2), 61-71.

Turekian, K.K., 1977. The fate of metals in the oceans. Geochim Cosmochim Acta 41, 11-39.

Vazquez-Ortega, A., Perdrial, J., Harpold, A., Zapata-Rios, X., Rasmussen, C., McIntosh, J., Schaap, M., Pelletier, J.D., Brooks, P.D., Amistadi, M.K., Chorover, J., 2015. Rare earth elements as reactive tracers of biogeochemical weathering in forested rhyolitic terrain. Chemical geology 391, 19-32.

Veyland, A., Dupont, L., Pierrard, J.C., Rimbault, J., and Aplincourt, M., 1998. Thermodynamic stability of zirconium(IV) complexes with hydroxyl ions. European Journal of Inorganic Chemistry 641 (11), 1765-1770.

Voigt, M., Mavromatis, V., and Oelkers, E.H., 2017. The experimental determination of REE partition coefficients in the water-calcite system. Chemical Geology 462, 30-43.

Volkova, A.V., Ermakova, L.E., and Golikova, E.V., 2017. Peculiarities of coagulation of the pseudohydrophillic colloids: Aggregate stability of the positively charged gamma-Al2O3 hydrosol in NaCl solutions. Colloids and Surfaces a-Physicochemical and Engineering Aspects 516, 129-138.

Wood, S. A., 1990. The aqueous geochemistry of the rare-earth elements and yttrium 1. Review of available low-temperature data for inorganic complexes and the inorganic REE speciation of natural waters. Chem. Geol. 82, 159-186.

Zhang J., Quay P. D., and Wilbur D. O., 1995. Carbon isotope fractionation during gas-water exchange and dissolution of CO_2. Geochim Cosmochim Acta 59, 107–114.

Appendix – 1

Tab. 4.1 – Main physical-chemical parameters and chemical composition of dissolved fraction (DF) samples expressed in mmol l^{-1}; DOC concentrations expressed in mg l^{-1}.

Sample	Remarks	pH	Eh (mV)	cond. mS cm^{-1}	T (°C)	Ionic Strength mol kg^{-1}	Na mmol	K mmol	Ca mmol	Mg mmol	Cl mmol	Br mmol	NO3 mmol	SO4 mmol	HCO3 mmol	DOC ppm
PL-1	*Stincone creek*	8.1	9.5	14.7	10.6	0.3	89.11	2.42	15.30	32.56	98.78			46.03	8.30	7.71
PL-2	*Stincone creek*	8.0	200.0	8.2	26.2	0.2	54.98	1.76	13.89	20.83	42.27			36.84	7.20	11.11
PL-3	*Stincone creek*	7.2	-16.8	114.2	14.7	3.1	2313.90	94.55	20.58	161.17	2300.00	2.85	45.28	186.71	5.60	10.07
PL-4	*Stincone creek*	7.8	156.8	12.0	20.4	0.3	139.65	5.14	15.29	29.35	125.46			49.64	4.93	6.42
PL-5	*Stincone creek*	7.8	-16.0	111.3	17.9	2.7	1990.21	78.73	21.58	133.39	2236.75	0.95	8.03	112.00	5.27	
PL-6	*Stincone creek*	8.1	-25.0	71.7	31.4	1.4	946.22	51.22	23.11	84.80	1042.17			79.05	4.40	
PL-7	*Stincone creek*	7.7	25.0	108.0	25.2	4.3	3070.4	121.6	20.6	246.5	3813.2			145.0	5.4	13.39
PL-8	*Salito creek*	8.0	43.8	28.0	19.2	0.4	281.8	5.3	20.1	17.4	299.9			29.7	3.3	5.0
PL-9	*Salito creek*	8.1	42.0	33.0	27.0	0.6	422.7	7.4	23.2	30.4	466.5			32.9	2.7	
PL-10	*Salito creek*	8.0	31.0	33.5	19.6	0.5	349.0	8.8	20.7	25.0	412.1			34.3	3.4	5.9
PL-11	*Salito creek*	8.1	142.0	61.0	26.2	1.5	1090.5	33.8	21.4	83.2	1280.9			65.9	3.3	
PL-12	*Salito creek*	7.0	31.8	20.1	24.3	0.4	222.6	5.3	20.8	16.4	228.7			31.6	3.8	5.04
PL-13	*Salito creek*	8.0	65.0	45.9	9.4	0.7	475.1	14.8	20.3	37.4	523.2	0.5		35.0	4.4	8.32
PL-14	*Salito creek*	8.0	-75.0	48.6	12.0	0.8	536.8	15.4	22.0	40.0	602.5	0.4		38.6	3.4	7.36
PL-15	*Belici creek*	8.3	85.0	5.8	20.4	0.1	39.8	0.6	5.0	3.6	34.8			8.4	5.9	7.9
PL-16	*Belici creek*	7.9	129.3	13.0	20.4	0.2	162.9	1.8	13.1	6.3	167.7			15.5	4.2	
PL-17	*Belici creek*	8.0	79.2	6.4	25.4	0.1	51.6		5.4	3.9	46.9			9.4	4.8	6.32
PL-18	*Salito creek*	8.3	57.7	15.8	21.8	0.2	159.4	3.5	10.2	10.0	160.4			17.1	4.5	6.16
PL-19	*Salito creek*	8.3	85.0	42.2	25.4	0.9	610.3	14.5	24.4	40.9	666.2			41.2	2.0	5.11
PL-20	*Salito creek*	8.0	-42.0	37.1	12.9	0.5	371.0	10.0	17.0	24.9	412.2	0.2		27.7	4.4	6.1
PL-21	*Salito creek*	8.0	34.0	35.9	11.8	0.5	368.9	8.6	16.5	21.0	410.4	0.2		27.0	4.3	
PL-22	*Fiumicello creek*	8.4	68.0	10.6	22.0	0.1	91.5	2.1	8.8	3.5	89.6			11.3	4.8	6.12
PL-23	*Fiumicello creek*	8.2	156.0	8.5	28.6	0.1	83.5	1.8	9.7	2.9	91.6		0.5	13.3	4.7	6.12
PL-24	*Fiumicello creek*	7.9	79.0	14.5	9.7	0.2	133.5	2.8	7.3	3.8	140.7			9.3	6.1	
PL-25	*Salito creek*	7.9	28.0	16.5	26.1	0.3	166.3	4.0	13.4	11.0	170.1			22.5	4.0	4.95
PL-26	*Salito creek*	8.6	42.0	14.9	20.5	0.2	153.8	3.4	9.8	8.8	157.1			16.5	3.1	9.3
PL-27	*Salito creek*	8.2	145.0	15.0	27.4	0.3	207.6	3.7	14.0	9.0	215.1		0.7	18.6	3.1	
PL-28	*Salito creek*	8.0	181.0	28.4	8.6	0.4	304.9	7.2	16.7	20.7	340.0			23.2	3.1	10.81
PL-29	*Gallo D'Oro creek*	8.0	38.0	22.3	8.5	0.3	234.5	5.5	13.7	15.5	258.9			19.3	3.1	6.25
PL-30	*Gallo D'Oro creek*	8.2	122.0	15.3	8.9	0.2	141.5	2.8	9.8	6.7	146.9			3.5	3.7	7.49
PL-31	*Gallo D'Oro creek*	8.0	124.0	15.0	7.5	0.2	137.1	2.8	10.4	6.8	143.7			13.5	4.7	7.16
PL-32	*Gallo D'Oro creek*	7.8	139.0	9.2	9.6	0.1	73.5	1.9	6.3	4.1	77.3			8.2	2.5	7.50
PL-33	*Platani river*	7.4	45.0	13.1	26.6	0.2	116.9	2.5	10.1	6.5	119.9			15.0	2.8	5.3
PL-34	*Platani river*	7.9	22.0	15.8	29.8	0.2	148.4	4.2	13.3	8.6	150.9			19.8	2.9	5.9
PL-35	*Platani river*	7.9	45.0	12.8	28.0	0.2	115.4	2.6	14.7	7.3	118.2			20.2	2.9	4.9
PL-36	*Platani river*	8.0	12.0	16.0	30.6	0.2	148.2	3.1	14.5	8.7	152.5			21.3	2.9	5.03
PL-37	*Platani river*	8.1	22.0	12.9	30.2	0.2	114.0	2.4	14.2	7.4	116.5			19.6	3.2	3.92
PL-38	*Platani river*	8.0	30.0	13.6	30.0	0.2	116.8	2.5	14.0	7.3	121.0			20.2	3.1	4.32

Appendix – 2

Tab. 4.2 - YREE, Zr and Hf concentrations of dissolved fraction (DF) samples expressed in pmol l^{-1}.

Sample	Remarks	Y	Zr	La	Ce	Pr	Nd	Sm	Eu	Gd	Tb	Dy	Ho	Er	Tm	Yb	Lu	Hf	ΣREE	Zr/Hf	Ce/Ce*	Gd/Gd*
PL-1	Stincone creek	149.6	383.7	80.6	209.1	21.3	90.8	21.3	4.6	19.7	3.1	14.8	3.0	7.8	1.2	6.9	1.1	1.7	485.4	228.3	1.2	0.9
PL-2	Stincone creek	160.8	235.7	554.3	466.0	22.7	89.4	20.6	5.3	21.6	3.1	15.4	3.0	8.4	1.2	7.5	1.1	2.2	1219.8	105.2	0.7	1.0
PL-3	Stincone creek	329.6	1051.3	78.5	146.3	11.4	55.5	10.0	2.6	15.3	2.5	14.2	3.6	12.0	1.8	12.7	2.3	3.4	368.5	312.7	1.1	1.1
PL-4	Stincone creek	158.6	349.7	533.5	394.0	13.5	55.5	13.3	3.3	14.0	2.5	12.3	2.4	7.8	1.2	5.8	1.1	3.4	1060.1	104.0	0.6	0.8
PL-5	Stincone creek	310.4	952.6	45.4	135.6	11.4	51.3	12.6	3.3	15.9	2.5	16.0	4.2	13.8	2.4	13.9	2.3	2.8	330.5	340.1	1.4	1.2
PL-6	Stincone creek	195.7	289.4	58.3	133.5	10.6	47.1	11.3	3.3	14.0	1.9	11.7	2.4	8.4	1.2	7.5	1.7	1.1	312.9	258.3	1.2	1.2
PL-7	Stincone creek	431.9	791.5	83.5	199.8	17.0	81.1	21.9	5.3	25.4	4.4	25.8	6.1	19.7	3.0	19.1	3.4	2.8	515.6	282.5	1.2	1.0
PL-8	Salito creek	208.1	100.9	51.1	115.6	12.1	54.1	12.6	3.3	21.6	2.5	14.2	3.6	12.6	2.4	16.8	3.4	1.1	325.8	90.0	1.1	1.5
PL-9	Salito creek	283.4	172.1	131.0	219.1	22.0	101.2	23.9	5.9	101.7	4.4	22.8	4.9	15.5	2.4	17.3	2.9	1.7	675.1	102.4	0.9	3.6
PL-10	Salito creek	183.3	127.2	26.6	52.1	4.3	20.1	6.0	2.0	14.6	1.3	9.8	3.0	10.2	1.8	15.0	3.4	0.6	170.2	227.0	1.1	2.7
PL-11	Salito creek	329.6	156.8	96.5	206.3	24.1	108.8	23.9	7.2	79.5	4.4	24.0	4.9	16.1	2.4	16.8	2.9	1.7	617.8	93.3	1.0	2.8
PL-12	Salito creek	555.6	291.6	629.2	886.4	77.4	330.7	81.1	18.4	90.3	11.3	52.3	10.3	26.9	3.6	23.1	4.0	3.4	2245.1	86.7	0.9	1.1
PL-13	Salito creek	861.6	1031.5	599.0	1184.7	141.2	565.7	139.7	34.2	134.2	20.1	92.9	21.2	51.4	8.3	47.4	7.4	13.4	3047.5	76.7	0.9	1.0
PL-14	Salito creek	475.8	530.6	232.5	583.1	67.4	324.5	88.5	18.4	84.6	12.6	57.2	10.9	33.5	5.3	33.5	5.7	N/A	1557.7	N/A	1.1	0.9
PL-15	Belici creek	237.3	213.8	46.1	128.5	16.3	71.4	16.6	5.3	26.7	3.1	18.5	3.6	13.2	1.8	14.4	2.9	1.7	368.4	127.2	1.1	1.4
PL-16	Belici creek	293.6	305.8	112.3	284.1	33.4	136.6	35.9	9.2	35.6	5.0	28.3	4.9	14.9	1.8	12.7	2.3	3.4	716.9	91.0	1.1	1.0
PL-17	Belici creek	1178.8	582.1	446.3	1391.0	188.8	829.2	206.2	47.4	194.6	26.4	128.0	22.4	56.8	7.7	43.3	6.9	10.6	3595.0	54.7	1.1	1.0
PL-18	Salito creek	239.6	413.3	40.3	117.0	13.5	61.7	14.6	3.9	25.4	2.5	16.0	3.6	12.0	1.8	15.0	2.9	2.8	330.3	147.5	1.1	1.8
PL-19	Salito creek	169.8	158.9	98.6	179.9	19.2	83.9	21.9	4.6	146.9	3.1	17.2	3.0	9.0	1.8	10.4	2.3	2.2	601.8	70.9	1.0	6.8
PL-20	Salito creek	466.8	462.6	194.4	653.7	100.8	416.0	113.7	26.3	104.3	14.5	69.5	12.1	35.9	5.9	33.5	4.6	7.3	1785.2	63.5	1.0	1.0
PL-21	Salito creek	275.6	268.6	120.2	324.7	53.2	196.9	56.5	13.2	59.1	8.2	36.3	7.3	22.7	3.6	24.3	4.0	3.4	930.2	79.9	0.9	1.0
PL-22	Fiumicello creek	115.9	52.6	20.9	32.8	2.8	13.2	3.3	1.3	13.4	0.6	8.0	3.0	12.6	2.4	19.1	4.0	N/A	137.4	N/A	1.0	6.9
PL-23	Fiumicello creek	497.2	169.9	233.3	564.5	66.7	303.0	71.2	18.4	120.2	12.0	56.6	10.9	34.1	5.3	42.2	8.0	2.8	1546.3	60.7	1.0	1.4
PL-24	Fiumicello creek	167.6	31.8	73.4	154.9	21.3	101.2	33.9	11.8	61.7	8.8	25.2	6.7	21.5	3.6	27.7	4.0	N/A	555.8	N/A	0.9	0.9
PL-25	Salito creek	217.1	149.1	156.9	259.8	24.1	106.1	25.3	5.9	36.9	3.8	18.5	3.6	12.0	1.8	12.1	2.3	1.1	669.0	133.0	1.0	1.4
PL-26	Salito creek	104.6	293.8	92.1	147.7	8.5	37.4	9.3	2.6	24.8	1.3	9.2	2.4	7.8	1.2	10.4	2.3	2.2	357.1	131.1	1.1	4.0
PL-27	Salito creek	897.6	258.7	344.1	1004.9	124.9	550.5	132.3	31.6	163.4	20.8	101.5	19.4	50.2	6.5	41.0	6.9	4.5	2598.1	57.7	1.1	1.1
PL-28	Salito creek	10850.8	2528.9	4149.6	13591.7	1846.6	8505.3	2220.7	522.5	2045.8	290.1	1321.8	232.2	527.9	70.4	356.0	57.7	45.9	35738.3	55.0	1.1	0.9
PL-29	Gallo D'Oro creek	5738.7	2453.3	2147.5	7633.7	1041.8	4769.8	1257.6	298.1	1149.8	169.9	750.8	135.8	304.9	33.1	215.0	28.6	48.7	19936.5	50.3	1.1	0.9
PL-30	Gallo D'Oro creek	3756.8	628.1	1452.8	4678.3	633.7	2884.1	746.2	181.0	745.9	102.6	462.2	87.9	193.1	26.0	134.7	20.0	12.3	12348.5	51.0	1.1	1.0
PL-31	Gallo D'Oro creek	455.5	112.9	219.6	532.4	76.6	311.3	83.1	25.0	122.7	17.6	56.6	10.9	31.7	5.3	31.8	4.0	1.7	1528.7	67.2	0.9	0.8
PL-32	Gallo D'Oro creek	6116.6	1058.9	2421.1	7758.6	1043.9	4694.3	1221.7	290.2	1128.1	165.5	743.4	137.0	306.1	37.3	220.2	31.4	18.5	20198.9	57.3	1.1	0.9
PL-33	Platani river	796.3	202.8	339.1	874.3	108.6	484.6	119.0	28.3	134.8	15.7	78.8	15.2	40.7	5.9	36.4	6.3	3.4	2287.6	60.3	1.0	1.2
PL-34	Platani river	1227.1	504.3	478.0	1329.6	171.7	756.4	182.9	42.8	188.2	24.5	121.8	22.4	61.0	8.3	49.7	8.0	9.0	3445.5	56.3	1.0	1.1
PL-35	Platani river	760.4	450.5	295.9	793.6	99.4	443.0	109.7	25.7	120.2	15.1	72.6	13.9	39.5	5.3	33.5	5.7	9.0	2073.2	50.3	1.0	1.1
PL-36	Platani river	1413.9	633.6	479.5	1514.5	203.0	900.6	224.8	51.3	225.8	29.6	144.6	26.1	68.8	8.9	54.9	8.6	11.8	3940.7	53.9	1.1	1.1
PL-37	Platani river	1696.2	766.2	645.0	1894.2	243.4	1078.1	271.3	60.5	258.8	34.6	168.0	30.9	78.9	10.1	60.1	9.1	13.4	4843.2	57.0	1.1	1.0
PL-38	Platani river	1985.2	1077.6	1378.6	2543.6	290.3	1241.7	292.6	68.4	297.6	39.0	194.5	35.8	92.7	12.4	72.8	10.9	19.0	6570.9	56.6	0.9	1.1

Appendix - 3

Tab. 4. 3 – REE, Zr and Hf concentrations of Colloidal Fraction (CF) and Truly Dissolved Fraction (TDS), expressed in pmol l^{-1} and relative derived parameters

Colloidal Fraction	Remarks	Y	Zr	La	Ce	Pr	Nd	Sm	Eu	Gd	Tb	Dy	Ho	Er	Tm	Yb	Lu	Hf	ΣREE	Zr/Hf	% CF
Sample																					
PL-1	Stincone creek	1232.4	4514.7	51.7	125.4	31.1	209.3	168.4	44.8	83.5	9.7	68.8	21.7	40.5	11.7	79.5	23.1	158.9	969.3	28.4	29.6
PL-3	Stincone creek	3144.0	5894.9	214.5	165.6	129.1	862.7	2177.3	497.7	1669.3	185.0	986.1	251.5	464.8	131.8	1231.9	177.0	940.1	9144.4	6.3	0.8
PL-5	Stincone creek	3650.4	6686.9	266.6	340.6	316.4	1989.9	1940.8	490.3	1517.9	213.4	1083.2	338.9	420.7	187.6	1130.8	227.3	1246.5	10464.5	5.4	1.5
PL-8	Salito creek	3351.1	4331.4	55.5	59.4	62.1	182.4	441.3	154.0	341.7	35.3	167.6	71.7	121.1	38.7	327.5	90.8	248.1	2149.0	17.5	7.9
PL-10	Salito creek	2553.0	3310.2	122.9	159.8	62.5	464.2	274.9	166.1	395.5	43.5	152.5	81.3	92.7	34.0	238.2	91.2	204.7	2379.4	16.2	2.6
PL-15	Belici creek	1337.8	2593.2	28.6	70.4	10.2	147.1	123.5	76.9	184.0	14.4	84.8		40.9	11.5	98.1	42.6	97.0	933.0	26.7	25.7
PL-18	Salito creek	1063.1	1545.0	118.6	245.8	40.4	317.9	303.8	66.6	248.3	23.3	82.1	21.2	41.0	22.4	167.9	19.0	137.3	1718.3	11.3	24
PL-22	Fiumicello creek	1356.4	2505.2	46.0	89.9	12.6	149.4	130.6	93.3	135.0	12.9	86.1	15.9	47.0	15.9	42.4	21.4	95.6	898.5	26.2	NA
PL-26	Salito creek	1374.4	1930.7	24.3	33.9	15.5	79.6	120.9	65.0	113.0	17.2	49.4	14.0	34.5	8.0	48.1	24.0	82.7	647.3	23.4	23.4

Truly Dossolved Fracton	Remarks	Y	Zr	La	Ce	Pr	Nd	Sm	Eu	Gd	Tb	Dy	Ho	Er	Tm	Yb	Lu	Hf	ΣREE	Zr/Hf	%TDF
Sample																					
PL-1	Stincone creek	6.9	154.2	2.5	4.8	0.4	1.5	1.3	0.2	0.9	0.1	0.5	0.2	0.3	0.1	0.5	0.1	0.5	13.5	293.2	70.4
PL-3	Stincone creek	303.4	260.0	57.4	112.0	8.9	43.0	7.8	2.0	12.6	1.8	12.6	2.9	10.2	1.5	9.9	1.6	1.6	284.2	157.8	99.2
PL-5	Stincone creek	244.6	96.8	22.3	42.4	5.7	28.0	6.9	2.0	8.4	1.5	10.5	2.4	8.4	1.3	9.5	1.6	0.5	150.8	187.3	98.5
PL-8	Salito creek	98.9	45.4	7.3	8.3	1.1	4.8	1.9	0.6	3.6	0.4	3.4	1.1	4.3	0.7	5.6	1.0	0.2	43.9	191.2	92.1
PL-10	Salito creek	159.9	51.2	12.2	13.1	1.9	10.1	2.8	0.9	6.4	0.9	6.6	1.8	7.3	1.2	7.7	1.3	0.5	74.1	111.6	97.4
PL-15	Belici creek	7.1	159.8	7.7	9.3	0.6	2.1	0.6	0.4	1.3	0.1	0.6	0.2	0.3	0.1	0.6	0.2	0.9	23.9	182.2	74.3
PL-18	Salito creek	172.6	20.9	44.8	125.5	16.5	72.8	23.8	4.4	18.8	2.4	13.2	2.7	9.3	1.5	12.3	2.4	0.5	350.5	41.4	76
PL-22	Fiumicello creek	16.3	48.3	10.6	16.8	1.3	6.4	1.9	0.7	2.6	0.3	1.4	0.3	0.9	0.2	2.1	0.4	0.5	45.8	104.8	NA
PL-26	Salito creek	26.9	37.1	9.2	16.7	1.7	7.1	2.7	0.8	3.8	0.3	2.0	0.4	1.5	0.2	2.4	0.4	0.4	49.2	84.8	76.6

Appendix – 4

Tab. 4.4 – YREE, Zr and Hf concentrations and related molar ratios of bottom sediment fractions expressed in µmol kg^{-1}: 1st) Exchangeable cations and Ca carbonates; 2nd) Easily reducible; 3rd) Moderately reducible; 4th) Residual/silicate.

	Y	Zr	La	Ce	Pr	Nd	Sm	Eu	Gd	Tb	Dy	Ho	Er	Tm	Yb	Lu	Hf	ΣREE	Zr/Hf
										µmol kg-1									Molar Ratio
Exchangeable cations and Ca Carbonates																			
PL1	10.93	0.18	5.10	10.64	1.55	6.97	1.52	0.43	1.58	0.21	0.83	0.16	0.43	0.05	0.28	0.04	0.004	29.8	43.8
PL3	6.41	0.18	3.87	7.71	1.24	5.63	1.18	0.36	1.17	0.15	0.55	0.10	0.27	0.03	0.17	0.03	0.002	22.4	117.7
PL5	6.38	0.20	3.70	7.28	1.13	5.30	1.15	0.32	1.09	0.14	0.51	0.10	0.24	0.03	0.15	0.02	0.002	21.2	87.3
PL8	8.84	0.16	4.68	9.63	1.51	7.09	1.63	0.45	1.56	0.20	0.75	0.14	0.34	0.04	0.20	0.03	0.002	28.2	87.0
PL10	8.36	0.15	5.57	10.10	1.67	7.15	1.41	0.40	1.37	0.19	0.66	0.12	0.35	0.04	0.25	0.03	0.002	29.3	96.2
PL18	11.27	0.11	5.46	10.59	1.70	7.34	1.52	0.47	1.53	0.21	0.84	0.16	0.42	0.05	0.29	0.04	0.002	30.6	44.8
PL26	9.00	0.08	4.68	9.72	1.52	7.06	1.62	0.54	1.61	0.19	0.75	0.14	0.34	0.04	0.22	0.03	0.002	28.5	33.4
Easily reducible																			
PL1	0.68	0.02	0.13	0.36	0.05	0.23	0.07	0.02	0.07	0.01	0.07	0.01	0.03	0.00	0.02	0.00	0.0002	1.1	96.9
PL3	1.95	0.06	0.68	1.46	0.15	0.68	0.15	0.22	0.17	0.03	0.14	0.03	0.09	0.01	0.08	0.01	0.0007	3.9	94.4
PL5	1.89	0.10	0.76	1.46	0.19	0.79	0.17	0.10	0.18	0.03	0.13	0.03	0.06	0.01	0.05	0.01	0.0008	4.0	117.5
PL8	1.47	0.11	0.54	1.11	0.14	0.63	0.14	0.14	0.14	0.02	0.10	0.02	0.06	0.01	0.04	0.01	0.0007	3.1	170.9
Pl10	1.90	0.05	0.72	1.43	0.18	0.80	0.16	0.12	0.20	0.03	0.11	0.02	0.07	0.01	0.05	0.01	0.0003	3.9	159.3
PL18	1.43	0.06	0.54	1.14	0.15	0.60	0.14	0.07	0.15	0.02	0.10	0.02	0.06	0.01	0.04	0.01	0.0001	3.0	520.3
PL26	1.69	0.06	1.05	1.67	0.16	0.66	0.12	0.16	0.16	0.02	0.09	0.02	0.06	0.01	0.03	0.01	0.0005	4.2	115.7
Moderately reducible																			
PL1	3.23	4.86	1.39	3.88	0.50	2.03	0.48	0.14	0.49	0.07	0.37	0.07	0.17	0.02	0.12	0.02	0.07	9.8	65.0
PL3	4.36	7.02	2.19	5.96	0.87	3.65	0.87	0.20	0.80	0.12	0.54	0.09	0.25	0.03	0.17	0.02	0.12	15.8	57.1
PL5	4.97	6.94	2.52	6.88	1.00	4.02	0.96	0.23	0.94	0.14	0.60	0.11	0.27	0.03	0.20	0.03	0.12	17.9	58.6
PL8	4.28	5.42	1.79	5.22	0.83	3.62	0.92	0.22	0.89	0.13	0.55	0.09	0.23	0.03	0.17	0.02	0.11	14.7	51.1
Pl10	1.98	2.97	0.68	2.10	0.24	0.99	0.24	0.07	0.26	0.05	0.21	0.04	0.11	0.01	0.08	0.01	0.04	5.1	75.4
PL18	0.99	1.10	0.31	1.03	0.13	0.55	0.14	0.05	0.15	0.02	0.11	0.02	0.05	0.01	0.04	0.00	0.01	2.6	86.1
PL26	4.92	5.05	2.03	6.15	0.93	3.99	0.99	0.25	1.00	0.15	0.63	0.11	0.28	0.03	0.18	0.03	0.09	16.7	58.6
Residual																			
PL1	2.73	1461.19	2.47	12.71	0.80	3.14	0.75	2.09	1.00	0.10	0.62	0.12	0.34	0.06	0.36	0.06	18.28	24.6	79.9
PL3	3.41	1416.59	2.35	8.34	0.72	2.69	0.53	0.31	0.52	0.08	0.41	0.06	0.22	0.03	0.19	0.04	18.85	16.5	75.1
PL5	5.96	1482.10	2.21	8.23	0.69	3.27	0.77	0.33	0.78	0.12	0.59	0.12	0.35	0.06	0.29	0.04	19.75	17.8	75.0
PL8	3.95	1531.99	2.52	13.93	0.88	3.57	0.84	0.40	0.72	0.08	0.49	0.09	0.29	0.04	0.27	0.03	20.08	24.1	76.3
Pl10	64.82	739.43	83.83	214.18	23.45	86.03	17.43	4.78	14.37	1.95	9.90	1.90	5.48	0.74	4.90	0.64	9.83	469.6	75.2
PL18	5.00	164.50	5.20	21.07	1.45	5.23	1.23	0.64	1.10	0.17	0.88	0.15	0.51	0.07	0.49	0.06	2.30	38.3	71.6
PL26	15.99	912.70	18.35	64.33	5.01	18.94	3.44	1.35	2.79	0.48	2.24	0.41	1.46	0.16	1.16	0.21	11.98	120.3	76.2

Appendix – 5

Tab. 4.5 – Saturation index of main mineral phases (carbonates, Al, Fe- oxyhydroxides, sulphates, halite).

Sample	Anidrite	Aragonite	Boehmite	Calcite	Celestina	Dolominte		Gibbsite	Goethtite	Gypsum	Halite
	$CaSO_4$	$CaCO_3$	AlO_2H	$CaCO_3$	$SrSO_4$	$CaMg(CO)_3$	$Fe(OH)_3$	$Al(OH)_3$	FeOOH	$CaSO_4{:}2H_2O$	NaCl
PL1	-0.4	1.1	2.5	1.3	-0.9	4.0	-0.7	2.4	4.6	0.0	-3.9
PL2	-0.2	1.2	1.5	1.4	1.4	4.1	0.5	1.3	5.6	-0.1	-4.5
PL3	0.6	0.7	NA	0.8	-0.9	1.9	-4.7	NA	0.6	0.8	-1.2
PL4	-0.3	0.8	NA	0.9	-1.0	NA	-0.5	NA	4.7	-0.1	-3.6
PL5	-0.5	0.5	NA	0.6	-1.1	3.2	-2.8	NA	2.4	-0.3	-1.3
PL6	0.6	1.0	0.8	1.2	-1.5	4.2	-1.2	0.6	3.9	-0.5	-2.0
PL7	-0.5	0.4	NA	0.5	-1.0	3.3	-1.9	1.0	3.3	-0.4	-0.8
PL8	-0.5	0.8	1.9	0.9	-1.0	2.9	-2.6	1.7	2.6	-0.2	-3.0
PL9	-0.4	0.9	NA	1.1	-1.0	3.5	-0.4	0.7	4.7	-0.3	-2.7
PL10	-0.5	0.8	NA	1.0	-1.1	3.2	-1.7	NA	3.5	-0.3	-2.8
PL12	-0.3	0.1	2.4	0.2	-1.0	1.5	-3.8	2.2	1.3	-0.2	-3.2
PL13	-0.7	0.7	2.1	0.8	-1.1	3.1	-0.7	2.0	4.7	-0.4	-2.5
PL14	-0.6	0.6	1.7	0.8	-1.1	3.0	-3.1	1.6	2.2	-0.3	-2.4
PL15	-1.1	1.1	NA	1.3	-1.2	3.5	-1.1	NA	4.2	-0.8	-4.6
PL16	-0.7	0.8	NA	1.0	-1.0	2.8	-0.6	1.8	4.6	-0.5	-3.4
PL17	-0.9	0.8	0.5	1.0	-1.2	3.0	NA	0.4	NA	-0.8	-4.4
PL18	-0.8	1.1	2.4	1.3	-1.2	3.7	1.0	2.2	6.1	-0.6	-3.5
PL19	-0.4	0.8	NA	0.9	-1.0	3.3	0.4	1.6	5.6	-0.3	-2.4
PL20	-0.7	0.8	2.3	0.9	-1.2	3.1	-2.3	2.2	3.0	-0.4	-2.7
PL21	-0.7	0.7	1.9	0.9	-1.1	3.0	-1.2	1.8	4.1	-0.4	-2.7
PL22	-0.8	1.3	NA	1.4	-1.3	3.6	-0.4	-1.1	4.7	-0.6	-3.9
PL23	-0.7	1.2	NA	1.4	-1.2	3.4	0.0	1.1	5.1	-0.5	-4.0
PL24	-1.2	0.6	1.0	0.8	-1.5	2.4	-1.4	0.9	4.0	-0.8	-3.5
P25	-0.5	0.9	1.3	1.0	-1.1	3.1	-1.2	1.1	3.9	-0.4	-3.4
PL26	-0.8	1.1	NA	1.3	-1.2	3.6	-0.6		4.6	-0.6	-3.5
PL27	-0.6	1.0	NA	1.2	-1.2	3.4	0.1	0.5	5.2	-0.5	-3.2
P28	-0.8	0.4	0.8	0.5	-1.3	2.3	-1.2	0.7	4.1	-0.4	-2.9
PL-29	-0.8	0.5	NA	0.6	-1.3	2.4	-2.7	NA	2.7	-0.5	-3.1
PL-30	-1.5	0.8	0.5	0.9	-1.9	2.8	NA	0.4	NA	-1.2	-3.5
PL-31	-0.9	0.7	0.9	0.8	-1.4	2.6	-1.2	0.8	4.2	-0.6	-3.5
PL-32	-1.2	0.1	1.8	0.2	-1.6	1.4	-1.3	1.7	4.0	-0.8	-4.0
PL-33	-0.7	0.2	1.0	0.3	-1.3	1.7	-2.9	0.8	2.2	-0.5	-3.7
PL-34	-0.5	0.8	0.5	0.9	-1.1	2.8	-1.6	0.3	3.4	-0.4	-3.5
PL-35	-0.4	0.8	1.7	1.0	-1.1	2.8	-0.4	1.5	4.7	-0.3	-3.7
PL-36	-0.5	0.9	0.2	1.1	-1.1	3.1	-1.4	0.0	3.6	-0.3	-3.5
PL-37	-0.4	1.1	1.8	1.2	-1.1	3.3	0.3	1.6	5.3	-0.3	-3.7
PL-38	-0.4	1.0	0.1	1.1	-1.1	3.1	-1.2	-0.1	3.8	-0.3	-3.7

Acknowledgement

I would like to express all my gratitude to my supervisors Prof. Paolo Censi and Dr. Salvatore Inguaggiato, for being my mentors in these three years and encouraging my research, allowing to grow as a researcher. Special thanks also to Prof. Pierpaolo Zuddas, for its presence and incredible critical sense without which I would not have achieved this results.

I would like to thank all the staff members of ICP-MS (I.N.G.V. National Institute of Geophysics and Volcanology of Palermo), Dr. Marcello Liotta Dr. Lorenzo Brusca, Dr. Segio Bellomo, for their patience, availability and assistance at any time. I really appreciated all your efforts and I learn so much from the analytical point of view.

A thanks to my family, my mother, my father, my brother for supporting me in any time and for all possible point of view; thank also to my special grand-mother, she always believed in me and in everything I did.

A special thanks also to all my friends for encourage me to cross every difficulties I met during this period. Lastly I would like to thank Salvo Picone, the most special and incredible person that I know, without him all the goals of my life would have been impossible.